EPRI | ELECTRIC POWER RESEARCH INSTITUTE

PCI Analyses and Startup Ramp Rate Recommendations for Westinghouse Fuel in Exelon PWRs

WARNING:
Please read the Export Control Agreement on the back cover.

Technical Report

PCI Analyses and Startup Ramp Rate Recommendations for Westinghouse Fuel in Exelon PWRs

1012915

Final Report, April 2006

EPRI Project Manager
K. Edsinger

ELECTRIC POWER RESEARCH INSTITUTE
3420 Hillview Avenue, Palo Alto, California 94304-1395 • PO Box 10412, Palo Alto, California 94303-0813 • USA
800.313.3774 • 650.855.2121 • askepri@epri.com • www.epri.com

DISCLAIMER OF WARRANTIES AND LIMITATION OF LIABILITIES

ORGANIZATION(S) THAT PREPARED THIS DOCUMENT

ANATECH Corporation

NOTE

For further information about EPRI, call the EPRI Customer Assistance Center at 800.313.3774 or e-mail askepri@epri.com.

CITATIONS

This report was prepared by

ANATECH Corporation
5435 Oberlin Dr.
San Diego, CA 92121

Principal Investigators
R. Montgomery
N. Jahingir
D. Sunderland

This report describes research sponsored by the Electric Power Research Institute (EPRI).

The report is a corporate document that should be cited in the literature in the following manner:

PCI Analyses and Startup Ramp Rate Recommendations for Westinghouse Fuel in Exelon PWRs. EPRI, Palo Alto, CA: 2006. 1012915.

PRODUCT DESCRIPTION

Fuel failures closely correlated with reactor power changes occurred in two Exelon PWRs. Analysis of the conditions in failed rods from one of these plants (Braidwood Unit 1) performed with EPRI's thermal-mechanical fuel rod performance code FALCON included a sensitivity study to identify the factors that contributed significantly to the failures. The findings of this investigation were then used to make recommendations for alternate startup profiles to minimize the risk of fuel failure during startup, particularly for Byron-2, which was the next scheduled startup in an Exelon reactor.

Results & Findings

FALCON code modeling of the nominal geometry of the fuel rod and its recorded power history yielded peak cladding hoop stresses comparable to those calculated for boiling water reactors (BWRs) that have experienced fuel failures by a pellet cladding interaction (PCI) mechanism. Unfortunately, the threshold failure stress for FALCON is not well defined for PWR operation, and any conclusions on the failure mechanism will need to wait for the results of the ongoing destructive (hot cell) examination of several of the Braidwood fuel rods. In the meantime, the FALCON code was applied to quantify relative differences in fuel rod response in a parametric study to identify the set of factors in the Braidwood startup that could have contributed to the fuel failures. It was found that the fuel rod conditions were relatively insensitive to prior-cycle coast-down and depressurization/temperature history. The conditions were also insensitive to the moderator temperature coefficient power maneuver. The most significant factors were the effect of initial ramp rate, in conjunction with the xenon swing and axial offset. Calculations were also performed with a missing pellet surface (MPS) condition. As expected, MPS increased the peak cladding stress. However, the possible role of MPS in these PWR failures will not be known until an ongoing hot cell exam is complete.

Challenges & Objectives

The primary objective of this study was to provide a more conservative startup sequence for Byron-2 in light of startup failures in Braidwood-1 and a mid-cycle failure in Braidwood-2. The calculations will also be used to support the ongoing hot cell investigation to determine the cause of the failures. Several technical challenges had to be surmounted to complete this study, including building a FALCON model for ZIRLO™ cladding and a helium release model for zirconium diboride (burnable absorber pellet coating).

Applications, Values & Use

The calculations summarized in this report are directly applicable to the Braidwood and Byron units modeled, and the results have already been used to modify the startup of one of these units. The results will also be valuable in interpreting the ongoing root cause investigation of failures from Braidwood Units 1 and 2.

At this time, it is difficult to deduce more generic conclusions on operational margins. Ultimately, the hot cell investigation is expected to provide the most relevant information on avoiding the types of failures experienced. However, these results do call attention to factors that can stack up to increase cladding stress during startup, particularly ramp rates and the xenon transient.

EPRI Perspective

The results of this work have already accomplished their first objective in providing guidance on ramp rates for the startup of Byron-2. This unit restarted in September 2005 without fuel failures, although it is impossible to know how much of this success can be attributed to the revised ramp rates. The calculations also identified the location and magnitude of the peak cladding stresses, providing a tool to guide the interpretation of the ongoing hot cell examination. Results from two failed rods and three sound sibling rods currently undergoing destructive examination are anticipated in late 2006. Depending on the findings from those examinations, further calculations may be performed.

Approach

After modifying the FALCON code to model the Westinghouse fuel design of interest, the project team ran about 40 cases to study the influence of a number of variables that could influence fuel reliability.

Keywords

Reactor Startup
Fuel Rod Failure
Pellet Cladding Interaction (PCI)
Cladding Stress
Cumulative Damage Index
PWR Ramp Rates
Xenon Transient
FALCON
Westinghouse OFA

ACKNOWLEDGEMENTS

The authors would like to acknowledge the many people that contributed directly or indirectly to this effort. In particular, the efforts of Erich Wurz and Brian Manges (Exelon), and Balendra Sutharshan and Charlie Beard (Westinghouse) in helping define the project scope, gathering operational and fuel design data for the calculations, and reviewing the project at a number of points along the way has made the outcome immeasurably better.

EXECUTIVE SUMMARY

An analysis of Pellet-Cladding Interaction (PCI) was conducted for the Braidwood and Byron reactors. This report contains the analysis results for two (2) rods from the Braidwood 1 Cycle 10 startup, three (3) failed and one non-failed rod from the Braidwood 1 Cycle 11 startup, three (3) rods from the Byron 2 Cycle 13 startup, and the Braidwood 2 Cycle 10 rod that failed during a mid-cycle power maneuver.

The calculated maximum cladding hoop stress results from the analysis of the Braidwood 1 Cycle 10 fuel rods were used as a baseline for a successful reactor startup, along with the Cumulative Damage Index (CDI) as a secondary reference. Based on the FALCON analysis results presented in the report, the higher duty operation and faster power ascension experienced in Braidwood 1 Cycle 11 increased the cladding hoop stresses and CDI relative to previous cycles. It has been shown that missing pellet surfaces increase cladding hoop stress. Furthermore, the occurrence of unfavorable fuel rod geometry variations within the tolerance specifications may also increase peak cladding hoop stress. The influence of rod internal pressures (initial pressurization, fission gas release, and He release for IFBA rods) was also considered. In general, however, the trend of increased rod internal pressure tended to reduce the ultimate clad stress level.

Given these considerations, the analysis of Exelon's initially planned startup profile for Byron 2 Cycle 13, i.e., 3%/hr (40-75%RP) - 2%/hr (75-90% RP) - 1%/hr (90-100% RP), may not have provided sufficient reduction of the cladding hoop stress when compared to the Braidwood 1 Cycle 10 rods. Using the FALCON analysis results, the following startup profile for Byron 2 Cycle 13 (assuming the fuel has the same margin to PCI (or MPS-assisted PCI) failure as the fuel in Braidwood 1 Cycle 11) was recommended to decrease peak cladding hoop stress:

- Unrestricted ramp rate below 40% of full power operation
- 3%/hr reactor power increase rate between 40% and 75% of full power operation
- 0.5%/hr reactor power increase rate between 75% and 100% of full power operation

In the event missing pellet surface (MPS) similar in size to that assumed in the FALCON calculation is identified as the failure mechanism in Braidwood 1 Cycle 11, the following reactor startup profile would be recommended for the Byron and Braidwood units to decrease peak cladding hoop stress for cores without MPS:

- Unrestricted ramp rate below 40% of full power operation
- 3%/hr reactor power increase rate between 40% and 75% of full power operation
- 1%/hr reactor power increase rate between 75% and 88% of full power operation

- 5 hour hold period at 88% of full reactor power
- 0.5%/hr reactor power increase rate between 88% and 100% of full power operation

Because local axial power increases associated with non-equilibrium Xe-induced reactivity variations may produce local ramp-rates that exceed the rate restrictions, axial power variations (AO) during the reactor startup should also be minimized to decrease the potential for PCI failure. The potential for PCI failure was shown to be insensitive to the moderator temperature coefficient power maneuver, the reactor coastdown at the end of the cycle, and the depressurization/temperature history, although the limiting rods may not have been studied.

Peak stresses calculated for the Braidwood 2 Cycle 10 rod were largely similar to those calculated for Braidwood 1 Cycle 11. In the case of the former, the stresses were driven by a Xe-induced power oscillation following a return to power after a load follow maneuver. The oscillation resulted in a net power increase of 1.4kW/ft over the previously conditioned level that, when combined with the higher local burnup (48 GWd/MTU) resulted in a significant level of stress. Interestingly, FALCON calculated the peak rod stress at the same elevation as a short axial crack discovered in the poolside examination.

CONTENTS

LIST OF FIGURES

LIST OF TABLES

1
INTRODUCTION AND BACKGROUND

During 2003, Exelon PWRs experienced fuel rod failure indications in three of their PWRs. Most of the fuel rod failures occurred during reactor startup following a refueling outage shortly after the unit had achieved full power operation. In the case of Braidwood 2 Cycle 10, the fuel rod failure occurred following a return to full power after a brief power reduction period. Each of these fuel rod failure events occurred coincident with a reactor power maneuver, thus raising the issue of whether the fuel rod power increase could have caused the cladding failure. Typically, cladding failures in PWRs have occurred by either grid-rod fretting or debris fretting where the effect of power changes is not significant. Of the possible failure mechanisms related to power changes, one of the most likely is Pellet-Cladding Interaction (PCI), a stress corrosion cracking (SCC) process. Historically, cladding failure by PCI has been observed mostly in BWR fuel rods or PWR rods ramped in test reactors that experience a large power increase combined with a rapid power ascension rate. However, in recognition that PCI failures are possible in PWRs, restricted power ascension procedures during PWR reactor startup are also followed.

During the Braidwood 1 Cycle 11 and Byron 1 Cycle 13 startup, an increase in reactor coolant activity was noticed. A post-irradiation examination at poolside during the refueling outage revealed a total of 4 failed assemblies in the Braidwood 1 unit and 1 failed fuel rod in the Byron 1 unit. Subsequent inspections confirmed that rods M16S-O5, M12S-B6, and M19S-L2 in Braidwood 1 Cycle 11 had in fact developed through-wall cladding defects. While assembly M36S was identified to have a failed rod, high magnification visual and eddy current inspections of suspected leaking rods did not reveal any indications of through-wall or secondary defects. The rod with the strongest UT indication from M36S (rod M14) was sent to the hot cell along with the other rods where it was examined and confirmed to be sound.

During the later part of Braidwood Unit 2 Cycle 10 operation, an increase in the reactor coolant activity was noticed following a return to 100% reactor power after operation at reduced power for plant maintenance activities. After completion of the cycle, poolside examinations confirmed a 0.5” axial crack at approximately the 21” elevation in the O5 fuel rod from assembly R36S. At the time of failure this twice-burnt fuel had an average burnup of 43.7 GWd/tU and a nodal burnup of 47 GWd/tU at the crack location. Preliminary visual examinations of this rod eliminate debris fretting and crud related failure mechanisms. As this failure occurred during the power ascension period following a reduced power operation, PCI (including missing pellet surface-assisted PCI) is a failure mechanism under consideration.

A number of changes with respect to power ascension strategies, power uprates, increased capacity factors, and increased fuel burnup have occurred on these units prior to the cycles that experienced the failures. Regarding power ascension, below the threshold power level, the maximum power ascension rate is typically 15%/hr, and above the threshold, the power ascension rate had a maximum of 3%/hr. These ramp-rate restrictions have almost eliminated

most of the hold times (periods of constant power) above 40% power for performing various surveillance procedures during startup.

Exelon Corp. is conducting a root cause evaluation to determine the likely cause of the fuel rod failures in their Braidwood and Byron PWRs. Because of their association with power maneuvers and a common location within high power assemblies (adjacent to a thimble tube), there is concern that these failures could be caused by some form of PCI. The operating mechanism could be a "classic" form of PCI or one enhanced by pellet or cladding defects where the PCI failure threshold is reduced by defective fuel pellets present in the fuel stack at the location of the high rate of local power change. Potential pellet defects include both missing pellet surface (MPS). Based on this analysis, if one or more of these failures are found to experience conditions associated with PCI failures then Exelon would likely revisit their power ascension procedures. It was also anticipated that the PCI failure potential might be exacerbated by power maneuvering related to moderator temperature coefficient (MTC) measurement, axial power swing due to xenon transition, or the rapid depressurization at the end of the previous cycle.

This report summarizes FALCON's assessment of the PCI failure potential of the Westinghouse 17OFA fuel during the Exelon's Braidwood 1 Cycle 11 startup and the Braidwood 2 Cycle 10 mid-cycle power maneuver. Section 2 summarizes the FALCON modeling approach used to calculate the evolution of the cladding stresses during both steady state operation and during the startup ramp or mid-cycle power maneuvers. Section 3 describes the analysis of the Braidwood 1 Cycle 11 failures, including the fuel rod selection, the power history and the analysis results. Also included in Section 3 are the analyses used to construct the modified power ascension guidelines for the Byron 2 Cycle 13 startup. Section 4 summarizes the analysis approach and the results for the Braidwood 2 Cycle 10 fuel rod M36S-O5 that failed during the mid-cycle power maneuver. Finally, Section 5 contains the summary and conclusions.

2
MODEL DEVELOPMENT AND FALCON ANALYSIS APPROACH

The FALCON fuel rod behavior code was used to perform the calculations discussed in this report. FALCON is a state-of-the-art fuel rod behavior analysis code developed by EPRI to analyze the steady state and transient behavior of light water reactor fuel rods throughout the lifetime of the fuel [1]. FALCON is based on the finite element analysis (FEA) approach coupled with a complete set of thermal and mechanical material properties models that describe the effects of irradiation on the performance of UO_2 and Zircaloy cladding. FALCON has been used to calculate the steady state performance of power reactor rods up to 70 GWd/tU and the transient behavior of test reactor rods. A special capability of FALCON is the ability to use local effects models to calculate such conditions as cladding stress concentrations during power maneuvers. The versatile geometric modeling capability of FALCON allows for explicit representation of the missing pellet surface within the local effects PCI model. The fuel rod analysis is performed using two axisymmetric two-dimensional models, one with R-Z geometry (assumes azimuthal or circumferential uniformity in thermo-mechanical behavior) and an R-θ geometry (assumes axial uniformity in thermo-mechanical behavior). The R-θ geometry model enables analysis of the cladding stress and strain distributions with more detailed pellet-cladding mechanical interaction effects than the larger full length R-Z fuel rod model. Models for a Westinghouse 17x17 IFBA fuel rod were constructed with detailed fuel design data supplied by Westinghouse.

In addition to the geometric mechanical model, a detailed power history which captures sufficient spatial and temporal power resolution to model both global and local conditions must be developed for a reliable PCI analysis. Westinghouse provided detailed steady-state and power ramp data which were used to construct the necessary power histories for the FALCON analyses.

Under long service, fuel pellets experience a complex history of cracking, relocation and crack healing which eventually leads to hard fuel-clad contact at low power levels (i.e., below the average rod power) at various locations along the fuel rod. When a relatively large increase in power is imposed on the region where fuel-cladding contact is achieved at low power, the resulting hoop stress can be high enough to cause failure by stress corrosion cracking. Considering this situation, two parameters are used in FALCON to evaluate the PCI failure potential; the inner cladding surface hoop stress and the Cumulative Damage Index. The inner cladding surface hoop stress is used because it provides a measure of the pellet-cladding mechanical interaction during a power maneuver. On the other hand, the Cumulative Damage Index (CDI), relates to the time at which the cladding is undergoing stress-induced damage caused by stress corrosion cracking.

FALCON does not have explicit ZIRLO™ cladding properties, however, with data supplied by Westinghouse, property models for ZIRLO™ creep and irradiation growth were developed using adjustment factors in conjunction with the appropriate Zircaloy-4 models. A representative ZIRLO yield strength of 90 KSI was used for this analysis [2].

The failed fuel rods analyzed in the project contained a unique burnable absorber, ZrB_2, which is placed as a thin coating on the fuel pellet outer circumferential surface (integral fuel burnable absorber, IFBA pellets). The neutron capture by B-10 produces He and Li atoms, which are initially entrapped in the ZrB_2 layer. Ultimately the He escapes to the fuel rod void volume, thus changing the fill gas quantity and rod internal pressure. A special model for the helium release from the ZrB_2 coated pellets was developed for FALCON based on information the release rate provided by Westinghouse.

FALCON uses a fuel relocation model that was derived from much older fuel designs with higher initial pressure and larger diameter pellets, and as a result, it was necessary to modify the linear power threshold to represent the modern Westinghouse fuel design.

The FALCON FEA models used in the analysis of the Braidwood and Byron rods, the fuel rod power history development, the basis of the CDI model, the model modifications for ZIRLO™ cladding and IFBA pellets, and the modification of the FALCON relocation model are discussed below.

2.1 Fuel Models (Full-length (R-Z) and Local PCI (R-θ))

Westinghouse furnished proprietary 17OFA fuel rod design data and characteristics to ANATECH [3]. The principal fuel rod design parameters used in the analysis are shown in Table 2-1.

Table 2-1
Westinghouse 17OFA Fuel rod parameters

Description	Value
Cladding outer diameter (inch)	0.360
Cladding inner diameter (inch)	ns
Cladding Material	ZIRLO™
Pellet outer diameter (inch)	ns
Radial gap (mils)	ns
Enrichment (%)	4.6-4.95
Fuel density [% of T.D.]	95
Internal gas pressure [He] (psig)	ns
Dished pellet	Yes
Fuel stack length (inch)	144.0
IFBA stack length (inch)	ns
IFBA loading (mg/inch)	~1.9-2.4

ns = not shown in report, but used in calculation

From these and other data, which are provided in reference [2], a full-length model (R-Z geometry), as shown in Figure 2-1, was constructed and used to analyze the selected Braidwood 1 and Byron 2 fuel rods with FALCON using the steady state and startup power histories. The full-length R-Z model analyses were used to identify the axial location with the highest cladding hoop stress, and also to determine the fuel-cladding gap condition for the more detailed local PCI analysis with the R-θ model.

Figure 2-2 and Figure 2-3 show the detailed PCI model using the R-θ geometry (30°), which with symmetry about the abscissa (0°) represents a 60° wedge of the fuel pellet and cladding. Previous sensitivity studies have shown that this model size is sufficient to eliminate any effects arising from the symmetry boundary conditions [4]. The conditions of the fuel pellet and cladding are taken at the axial elevation corresponding to maximum cladding hoop stress position in the full-length R-Z model. The R-θ model contains a crack in the fuel pellet on one boundary that causes a localized stress concentration in the cladding adjacent to the crack. The maximum cladding stress in this model occurs in element 73, as shown in Figure 2-2. Figure 2-3 shows a similar 30° R-θ slice with a missing pellet surface added.

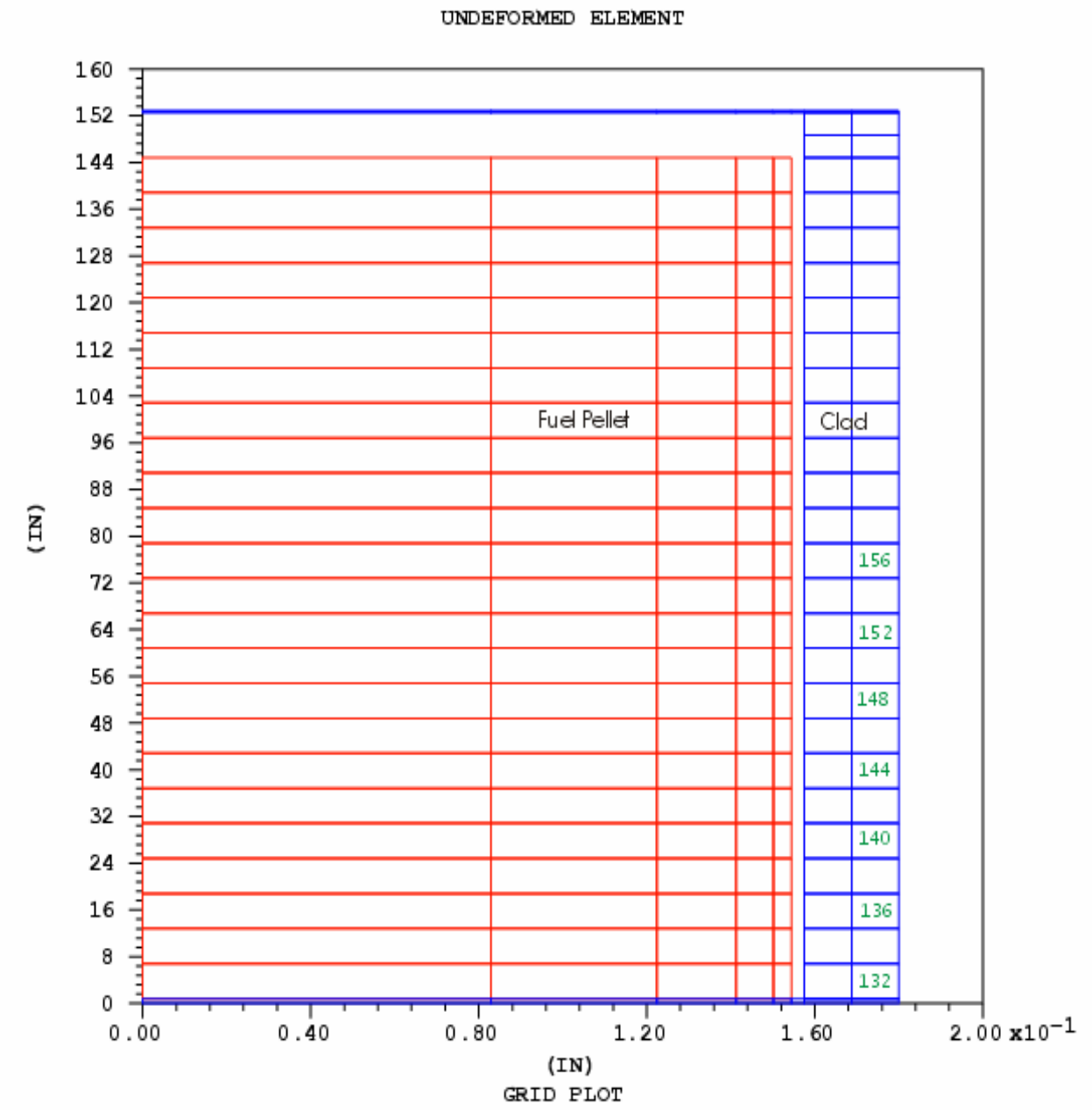

Figure 2-1
FALCON Full Length Fuel Rod Model in R-Z Orientation for Westinghouse 17OFA Fuel Rod

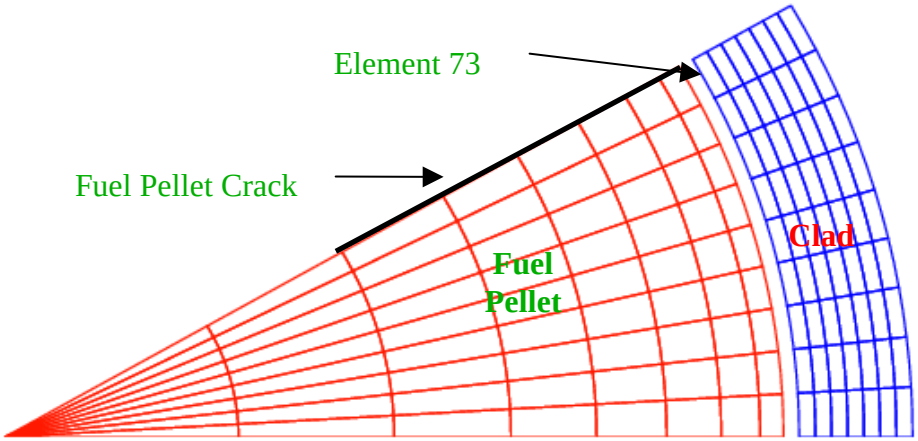

Figure 2-2
FALCON Fuel Rod Model in R-θ Orientation

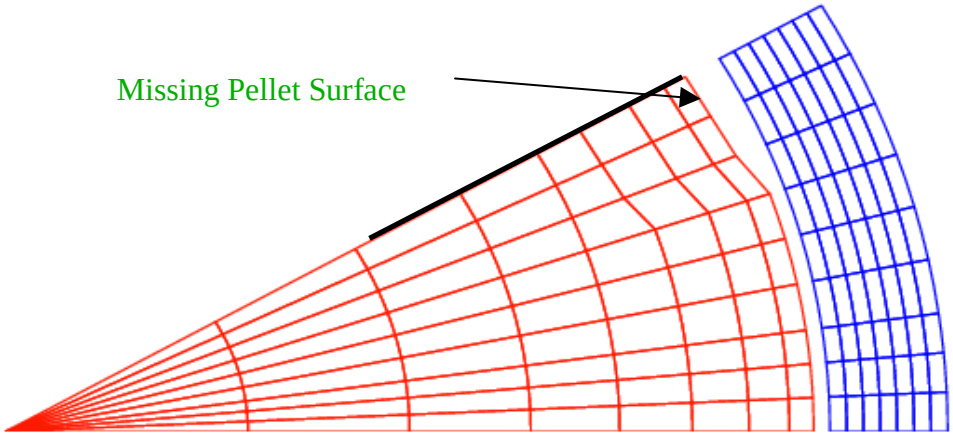

Figure 2-3
FALCON Fuel Rod Model in R-θ Orientation with a Missing Pellet Surface

2.2 Fuel Rod Power Histories and Operating Conditions

Fuel rod power history data and operating conditions were supplied by Westinghouse in the form of ANC output data files [5-7]. The data consisted of assembly axial factors, fuel rod radial peaking factors, core relative power factors, effective full power hours and burnup for each case/time step for the base depletion and startup ramp. Westinghouse also provided the fuel rod nodal scheme, pre- and post-uprated power for the Braidwood 1 and Byron 2 units.

ANATECH's in-house power history processing code RETRIEV was used to reconstruct the pin power history from these supplied core/assembly power data. This program extracts rod axial and radial factors, core relative power factors, as well as the EFPH for each time step/case based on the assembly and rod location from the supplied ANC output file. Since the axial factors in the supplied data are not normalized to 1.0, the axial factors are renormalized as follows:

$$\text{Normalized Axial Factors, } P_{(z,t)} = \frac{\sum AXLFAC_{(z,t)} * SEGHT_z}{Fuel\ Stack\ Length}$$

where, $AXLFAC_{(z,t)}$ is the rod axial factor at elevation z and time t, and the $SEGHT_z$ is the corresponding segment height. The normalized axial factors along with the supplied pre/post-uprated powers were used to reconstruct the rod average and local/nodal power as follows:

Rod Average Power,

$$PAVG_{(t)} = RADFAC_t * CORFAC_t * Cycle\ Avg.\ Power_t$$

Nodal Power,

$$PLOC_{(z,t)} = P_{(z,t)} * PAVG_t$$

where, $RADFAC_t$, $CORFAC_t$, $Cycel\ Avg.\ Power_t$ are the fuel rod radial factor, core relative power factor and core average linear heat rate at time t respectively. Figure 2-4 presents the RETRIEV calculated fuel rod average power and nodal peak powers as a function of EFPH for the D5 rod during the Braidwood 1 Cycle 9 base depletion. The supplied pre- and post-uprated power history files were added together to construct the Cycle 9 power history.

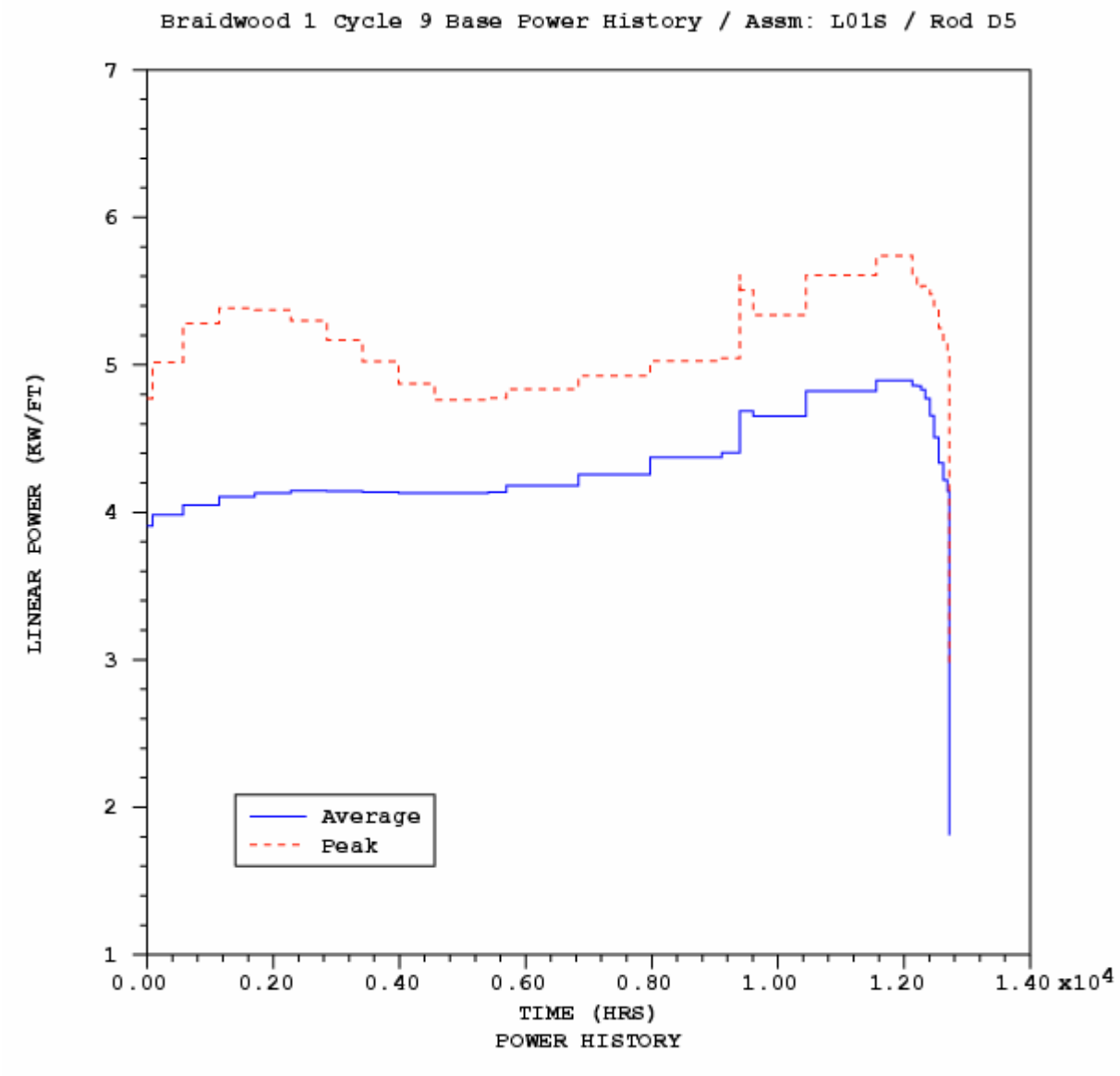

Figure 2-4
Base Depletion Power History for the D05 Rod during the Braidwood 1 Cycle 9 (without the MTC Measurement)

2.3 Cumulative Damage Index (CDI)

The phenomenon of PCI is highly stochastic and the prediction of failure under a set of conditions becomes a statistical problem. The model used to calculate the potential for cladding failure in FALCON is the cumulative damage index (CDI), which is based upon a time-temperature-stress model derived from stress-corrosion cracking (SCC) data as described below. The concept rests upon the assumption that the cladding material accumulates damage due to a sustained or repeated stress in the presence of SCC environment: the higher the stress, the shorter the time to failure. In FALCON, the incremental change in the Cumulative Damage Index (CDI), ΔD during a time increment Δt is given by;

$$\Delta D = \frac{\Delta t}{t_f(\sigma, T, \Phi)}$$

where t_f is the time to failure of Zircaloy by intergranular stress corrosion cracking (ISCC), provided the hoop stress (σ), temperature (T) and fast neutron fluence (Φ) levels remain unchanged during the time interval. Out-of-pile tube burst tests on unirradiated and irradiated Zr-4 and Zr-2 tubing has been used to develop the time to failure data as a function of these variables [8]. The total accumulated Damage Index at time t is given by;

$$CDI = D(t) = \int_0^t \Delta D dt$$

The function assumes that damage may accumulate only above a local burnup (B) of 5 GWD/MTU and when the cladding stress exceeds a threshold value, σ_{th} which is given by:

$$\sigma_{th} = 310.275\ (B - 5000)^{-0.0440} \qquad \text{for Zr-4}$$

where B is in MWD/MTU and σ_{th} is in MPa.

The threshold stress for initiation of PCI failure assumed in the FALCON model is 203 MPa (29.5 ksi) at a burnup level of 20 GWd/MTU. In FALCON, the CDI is calculated only when the local cladding stress exceeds the threshold stress given above.

2.4 FALCON Model Modifications

A method was developed to represent key ZIRLO™ cladding mechanical properties in the FALCON fuel behavior code. The approach consisted of applying multiplication factors on several Zircaloy-4 properties built-in to the FALCON material properties package. These key properties included: cladding irradiation creep and axial elongation rate. Westinghouse provided the data necessary to develop these methods [9]. In FALCON the creep equation for Zr-4 was modified for ZIRLO by multiplying the creep rate by a constant factor (the same factor was used for both thermal and irradiation creep). Since the actual thermal creep rate for ZIRLO is known to be higher than the value used in the FALCON calculations, the calculated cladding stresses during the power ascension would most likely be lower that those shown in this report. However, the actual thermal creep rate used in this analysis is not crucial since this is a comparative study. Similarly, the irradiation axial growth model of Zr-4 has been modified by multiplying the axial growth rate of Zr-4 by another factor. A representative yield strength of 90 ksi was used for this analysis [2].

An important element of this analysis is the helium release from the ZrB_2 coated pellets used in the Integral Fuel Burnable Absorber (IFBA) rods. Release of He into the rod internal volume increases the rod pressure and decreases the rate of pellet cladding gap closure. This factor in turn has an impact on the cladding stresses during a power ramp. ANATECH developed a boron depletion/helium release model based on the Westinghouse supplied data. The helium release has been modeled as a function of B_{10} loading and rod burnup. The L-assemblies have an U^{235} enrichment of 4.8 w/o and approximate IFBA loading 1.9 mg/in. The M-assemblies have an U^{235} enrichment of 4.95 w/o and a higher IFBA loading, approximately 2.4 mg/in. FALCON calculated helium release in terms of moles of helium and this compared well with the Westinghouse model [10].

The FALCON fuel relocation model calculates the change in pellet outer diameter caused by pellet relocation during steady-state operation. The model considers the effects of power, as-fabricated pellet diameter, as-fabricated gap thickness, and burnup. The model was developed from pellet mean-diameter measurements on fuel rods operated at power level between 8 and 22 kW/ft and to burnup levels between 0 and 11.5 GWd/tU. For this analysis, the default threshold power for initiation of fuel relocation was decreased from 6 kW/ft to 4 kW/ft to address the phenomenon of fuel deconditioning following extended low power operation. This modification has only a minor effect on the calculated pellet-cladding gap for rods operating at power levels well above 7 kW/ft, such as rods M14, B6 and L2, because these rods operated above the original threshold power of 6 kW/ft used to activate the model. (Sensitivity studies were used to verify that the impact of changing the threshold power in the relocation model was minimal for rods operated above 7 kW/ft.) The impact is largest on the fuel rods that operated for extended periods below 6 kW/ft during their first cycle of operation, such as the O5, M4, and D5 rods. Even with this modification, the calculated pellet-cladding gap remains open throughout the entire first cycle for both the O5 and D5 rods. The fuel relocation calculated by this model is applied incrementally within FALCON. Once the gap is closed no further relocation is considered unless gap reopening occurs at a later time. This model does not consider the recovery of relocation following gap closure.

2.5 FALCON Analysis Approach

The fuel rod analysis effort consists of three main steps that together are used to identify the effect of power operation on the PCI behavior of irradiated fuel. First, a steady state R-Z depletion analysis of the highest duty fuel, or a fuel rod of interest, e.g. one with a known failure, is performed to establish the fuel rod conditions at the end of the first cycle of operation. The result of the steady state analysis provides the initial fuel rod conditions used in the startup power ramp or mid cycle power maneuvering analysis. This analysis is performed with a power history from beginning of life to the point at which the power ramp or transient of interest occurs.

The second step of the analysis activity consists of a full length R-Z analysis of the power ramp. The cladding location with the maximum hoop stress is identified from the R-Z power ramp analysis. The power history used in this part of the analysis has much finer time resolution than the steady-state analysis.

In the third step, the local cladding stresses and PCI damage index response are calculated using the R-θ local effects model at the peak stress location. For the analysis of the Braidwood and Byron failures, the power ramp histories were modified for different hold times and ramp rates as part of a sensitivity analysis in order to evaluate potential reductions in stress and Cumulative Damage Index.

The results of the steady-state (R-Z) analysis and those of the power ramps using both the R-Z model and of the local effect PCI (R-θ) model are presented in Sections 3 and 4. The results are discussed in terms of the cladding stress and Cumulative Damage Index.

.

3
BRAIDWOOD 1 FUEL FAILURE ANALYSIS AND BYRON 2 STARTUP ANALYSIS

3.1 Candidate Rod Selection

One of the main objectives of this analysis was to determine the influence of the planned plant startup procedure on the Braidwood 1 Cycle 11 failures considering the actual fuel rod power histories. To provide a baseline comparison point, four (non-failed) rods were identified as reasonably representative of the limiting rods inserted in Braidwood 1 Cycle 9 and experiencing the startup during Cycle 10. These rods came from assemblies L01S and L08S and the changes in nodal power and rod average burnup are shown in Figure 3-1 and Figure 3-2, respectively. Two of these rods, M04 and D05 from assembly L01S, were judged to have experienced the most limiting combinations of burnup and power change between the Braidwood 1 Cycle 10 startup and Cycle 9 after coastdown. The analysis of these rods was included in the overall matrix to compare the magnitude and duration of the tensile stress with the failed and non-failed rods of the Braidwood 1 Cycle 11 startup and identify any increase in the PCI failure potential due to the changes in the startup procedure.

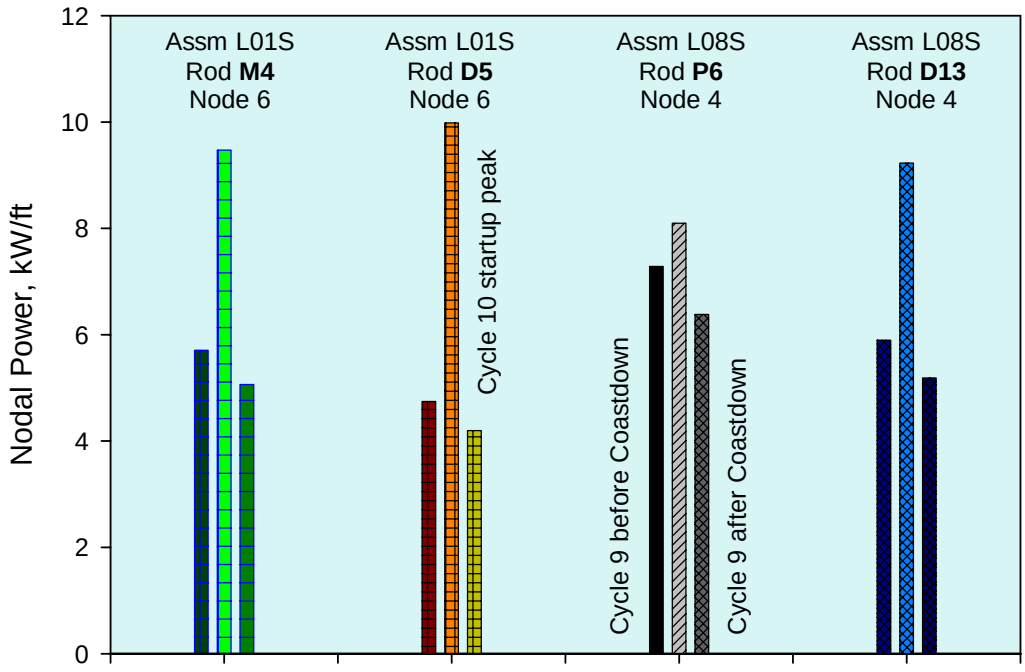

Figure 3-1
Fuel Rod Nodal Power Change during Braidwood 1 Cycle 9 and 10

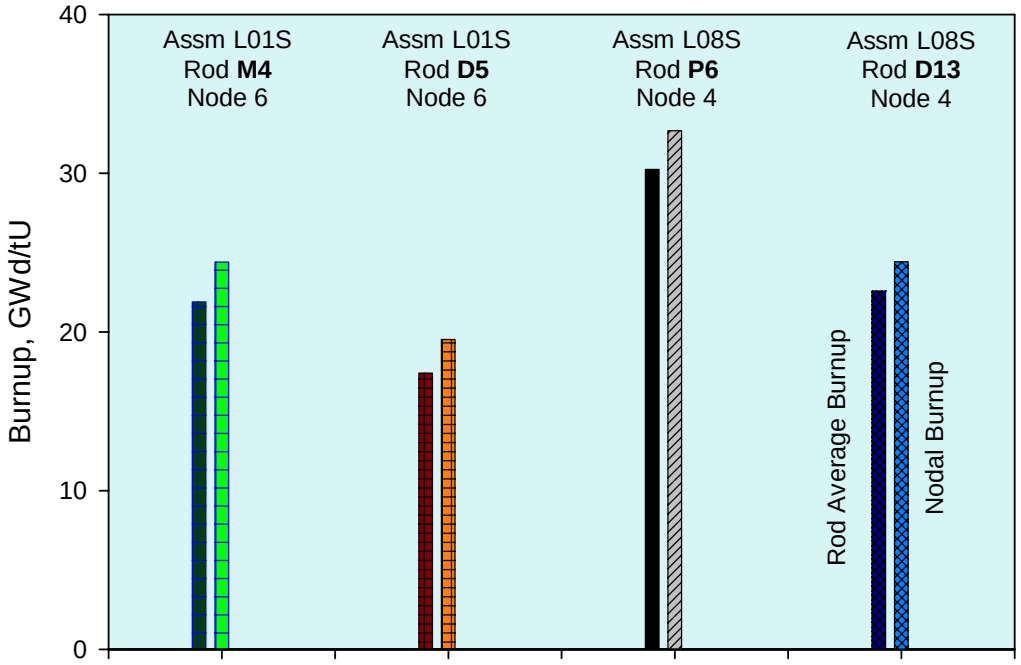

Figure 3-2
Fuel Rod Burnup during the Braidwood 1 Cycle 9 Base Depletion

For the Braidwood 1 Cycle 11 analysis three failed rods O5, B6, and L2 from assemblies M16S, M12S, and M19S, respectively and a non-failed rod M14 from assembly M36S were analyzed with FALCON. While rod M14 from assembly M36S has been confirmed to be non-failed, assembly M36S was identified to contain a leaking fuel rod. Without further information about the leaking rod, the M14 rod used in the analysis described in this report will be considered a surrogate for the failed rod for purposes of the PCI failure evaluation. The nodal power change for these rods, as well as the nodal and rod average burnup, is shown in Figure 3-3 and Figure 3-4 respectively. Similarly, for the Byron 2 Cycle 13 startup analysis, two rods C7 and D13 from the T30E assembly and one rod M14 from the T13E assembly were selected. These rods have experienced similar power changes and have comparable burnup to the Braidwood 1 cycle 11 failed rods. The nodal powers and rod burnups are shown in Figure 3-5 and Figure 3-6, respectively.

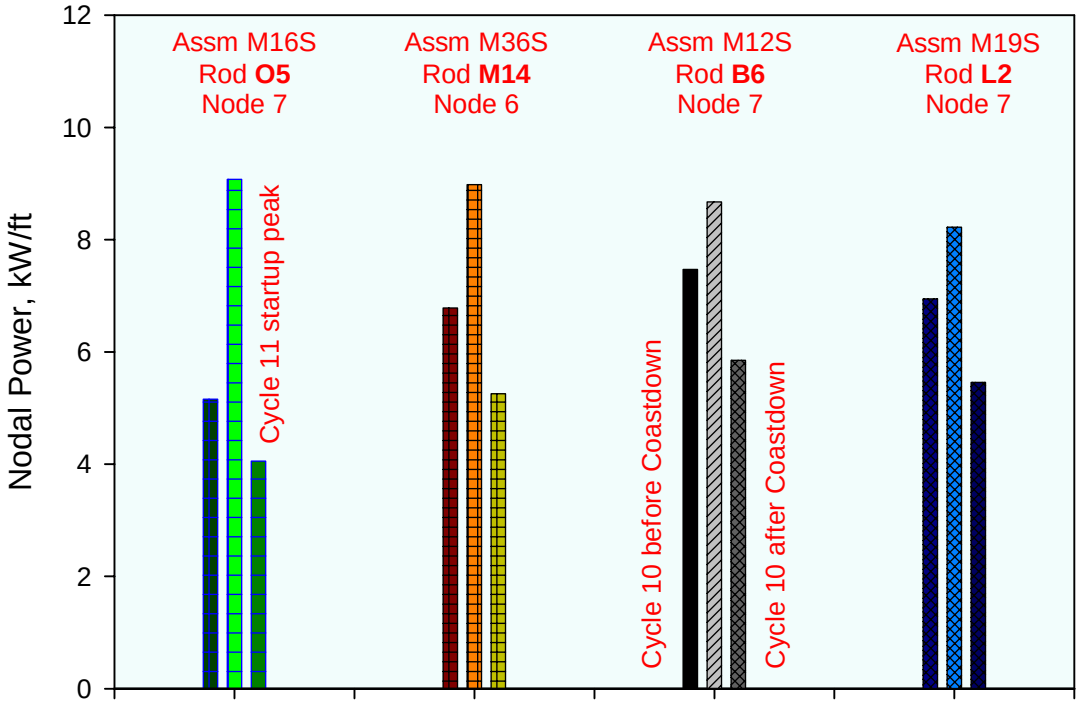

Figure 3-3
Fuel Rod Nodal Power during Braidwood 1 Cycle 10 and 11

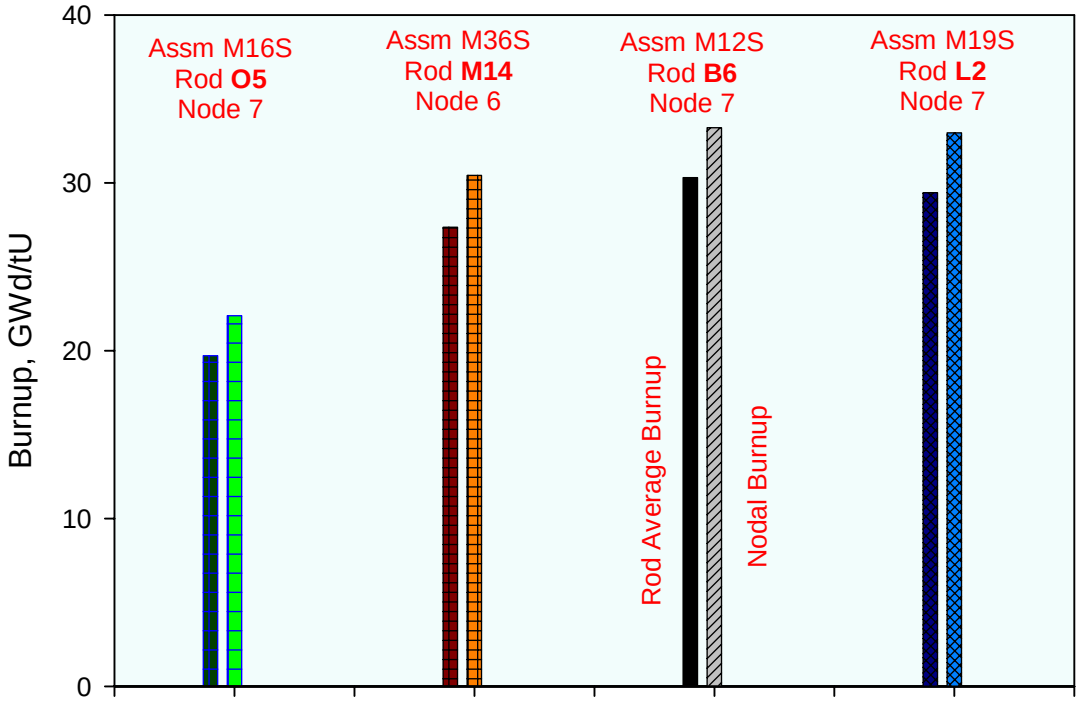

Figure 3-4
Fuel Rod Burnup during the Braidwood 1 Cycle 10 Base Depletion

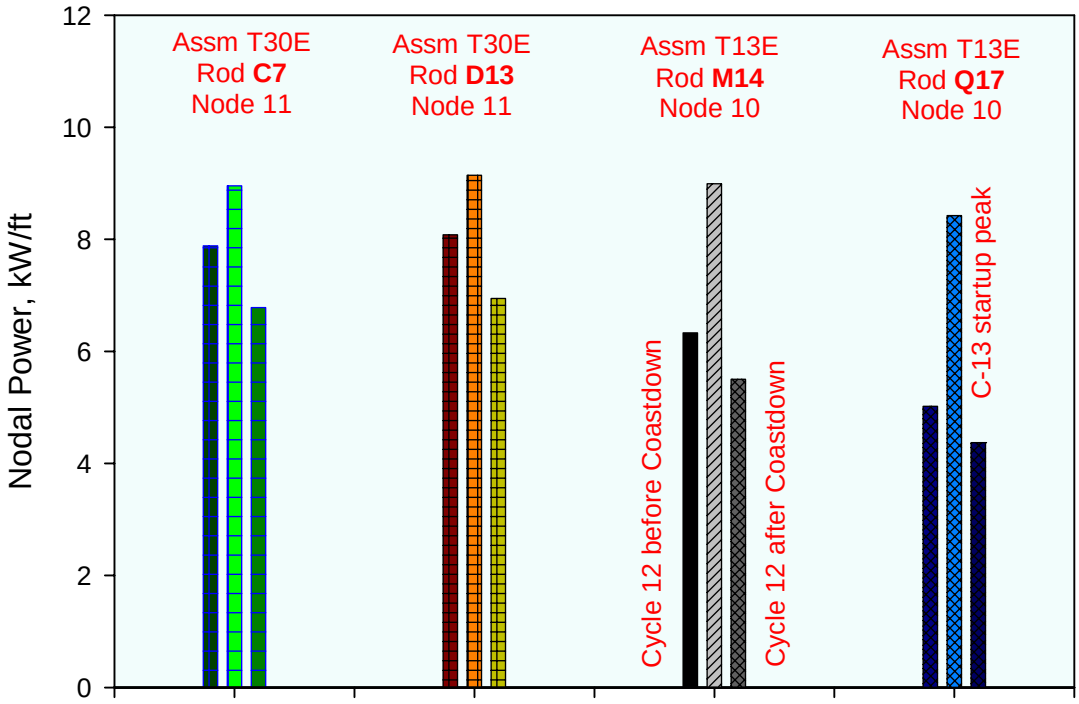

Figure 3-5
Fuel Rod Nodal Power during Byron 2 Cycle 12 and 13

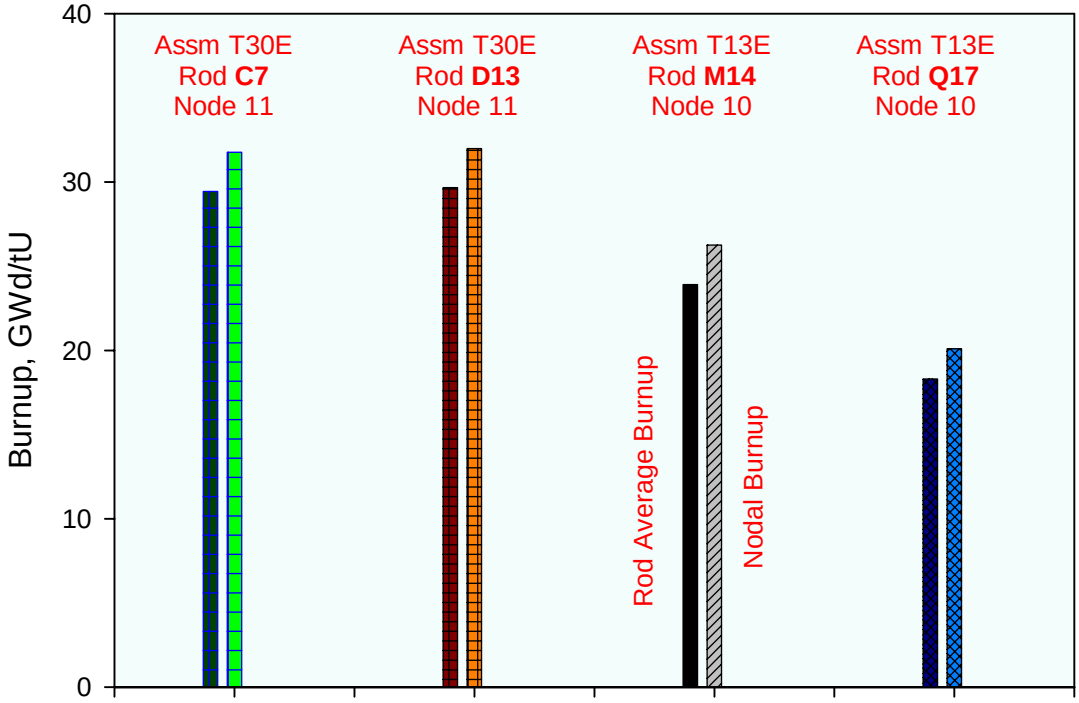

Figure 3-6
Fuel Rod Burnup during the Byron 2 Cycle 12 Base Depletion

3.2 Steady-State Analysis to Initialize Fuel Rod Conditions for Startup Ramp Analysis

In the first task of this analysis, the steady-state operation of fuel rods M04 and D5 during Braidwood 1 Cycles 9 was modeled with FALCON using a full-length fuel rod model with the R-Z geometry (Figure 2-1). The results of the steady-state analysis established the initial conditions (e.g. fuel-cladding gap, fission gas release, rod internal pressure, initial cladding stress) for the analysis of the next cycle startup ramp, which were also performed with the full-length R-Z fuel rod model. For the M04 rod the base irradiation power history has been modified to determine the effect of MTC measurement and coastdown on cladding stress during the next cycle startup. Similarly, the base irradiation analysis of the four Braidwood 1 Cycle 11 failed and a non-failed rod have been performed with FALCON using the full-length R-Z model to determine the conditions of the fuel rods prior to the second cycle startup. One additional base irradiation (Braidwood 1 cycle 10) analysis was performed for the O5 rod of the M16S assembly to determine the influence of a worst-case tolerance stackup (minimum fuel rod gap) on the magnitude and duration of the clad tensile stresses and on the potential of PCI failure. For the selected Byron 2 rods, the base irradiation analysis was performed using the FALCON full length R-Z model and Byron 2 Cycle 12 depletion power histories. Table 3-1 and Table 3-2 summarize the rods used in this study and the base irradiation and startup ramp analysis case matrix, respectively.

Table 3-1
Summary of Braidwood 1 and Byron 2 Rods used in this Study

Plant	Assembly	Rod	Features
Braidwood 1	L01S	M4	Representative sound rods in cycle 10 startup
	L01S	D5	
	M16S	O5	Failed in cycle 11
	M36S	M14	Sound rod in cycle 11 startup
	M12S	B6	Failed in cycle 11
	M19S	L2	Failed in cycle 11
Byron 2	T30E	C7	Representative rods in subsequent cycle at Byron 2
		D13	
	T13E	M14	

3.3 Startup Ramp Analysis using Full-length (R-Z) and PCI (R-θ) Models

In order to identify the maximum cladding hoop stress location during the startup ramp a full-length FALCON R-Z analysis was performed for the selected fuel rods using the respective startup power histories. FALCON's versatile and highly user-oriented restart capability was used to retrieve the necessary data from the full-length base irradiation analysis. With this approach, the magnitude and axial location of peak cladding stress were identified during the startup ramp. The results for the startup ramp analysis were then used as input to the local effects PCI analysis. The special local PCI model uses a R-θ geometry to analyze the cladding stress in much greater detail than the R-Z model. The R-θ model (Figure 2-2 and Figure 2-3) is independent of the R-Z model, and whereas the startup ramp cases for the R-Z model can be initialized directly from the steady-state case output, the power ramp analyses using the R-θ model must be initialized independently. In this case, the initialization begins at zero power followed by a period of low power, e.g., at the base power of the ramp in order to match the initial conditions of power, and stress and strain.

The PCI analysis of the Braidwood 1 Cycle 10 startup was performed for the non-failed rods M4 and D5 to provide a basis for comparing the cladding stress and Cumulative Damage Index. Such an approach provides a method to estimate the increase in the PCI failure potential of the Braidwood 1 Cycle 11 failed rods due to the change in the power ascension procedure. For the M4 rod the nodal startup power history has been modified to determine the impact of axial power swing due to the xenon transition. For this analysis a constant axial shape was assumed after the fuel rod reached 85% of the rod average power at the end of the startup ramp. In addition to the Braidwood 1 Cycle 11 PCI analysis of the failed rods using nominal pellet and cladding dimensions, one additional PCI analysis was performed for each of the O5 and M14 rod to determine the impact of the missing pellet surface on the potential for the cladding failure. Table 3-3 summarizes the missing pellet surface dimensions used for this analysis. The missing pellet surface geometry was determined by scaling a known pellet defect, which had caused the failure of an 8x8 BWR fuel rod in the KKL reactor [11]. For the Byron 2 fuel rod analysis, the PCI analysis was performed with the as-supplied startup power as well as with modified startup ramps and the results are compared with the Braidwood 1 Cycle 11 failed rods. ANATECH worked with Exelon to determine the best options both in terms of fuel reliability and plant feasibility to modify the Byron 2 Cycle 13 startup profile to minimize the PCI failure potential. The results of the analyses with the R-Z and R-θ model are discussed in the following sections.

Table 3-2
Braidwood 1 and Byron 2 Fuel Failure Analysis Case Matrix

ASSM	Fuel Rod	Analysis Approach	BD1 C9 Base	BD1 C10 PCI	BD1 C10 Base	BD1 C11 PCI	BY2 C12 Base	BY2 C13 PCI
L01S	M4	CD(+), MTC(+)	x	**x**				
		CD(-), MTC(+)	x	**x**				
		CD(+), MTC(-)	x	**x**				
		CD(-), MTC(-)	x	**x**				
		CD(+), MTC(+), AO(+)		**x**				
		CD(+), MTC(+), AO(-)		**x**				
L01S	D5	CD(+), MTC(+), AO(+)	x	**x**				
M16S	O5	minumum initial gap			x	**x**		
		50% Helium Release			x	**x**		
		baseline			x	**x**		
		depressurization			x	**x**		
		nominal chip				**x**		
		extended hold time				**x**		
M36S	M14	baseline			x	**x**		
		Nominal chip				**x**		
M12S	B6	baseline			x	**x**		
M19S	L2	baseline			x	**x**		
T30E	C7	baseline					x	**x**
T30E	D13	baseline					x	**x**
		8 hr hold@ 88% Power						**x**
		8 Hr hold @ 75, 88 & 95% Power						**x**
		8 Hr hold @ 88% & 95% Power						**x**
		8 Hr hold @ 88% & 50% slower ramp from 88% to 98%						**x**
		5 Hr hold @ 88% & 50% slower ramp from 75% to 98%						**x**
		1 hr hold @ 88 % & 0.5%/hr ramp from 75 to 98%						**x**
T13E	M14	baseline					x	**x**

Table 3-3
Missing Pellet Surface Dimensions

Description	Value
Width (inch)*	0.079

* This is the value used for the KKL analysis – the width used in this analysis was scaled from this value by the ratio pellet diameters

3.4 Braidwood 1 Fuel Failure Analysis Results

The steady-state fuel rod nodal power histories corresponding to the peak stress location during the Braidwood 1 Cycle 9 and 10 base irradiations are plotted in Figure 3-7. Two of the three failed rods L2, B6 and non-failed rod M14 experienced about 2 kW/ft higher nodal power during the Cycle 10 base irradiation than the two Cycle 9 non-failed rods. As a consequence these three rods (L2, B6, and M14) accumulate higher rod average and nodal burnup, which is reported in Table 3-4 and Table 3-5. However, these three rods (L2, B6, and M14) have experienced comparatively lower power change during the Cycle 11 startup than the other failed rod O5. Fuel rod O5 has comparable nodal burnup to the two Cycle 9 non-failed rods and experienced the largest change in power between the Cycle 11 startup and the Cycle 10 coastdown power. As the L2, B6 and M14 rods have experienced higher nodal power during the Cycle 10 base irradiation, the pellet-cladding gaps for these rods closes after about 350 EFPDs (within their first cycle) in the reactor. For the O5 and two non-failed rods M4 and D5, the pellet-cladding gap remains open during the base irradiations in Cycle 10 and 9, respectively. A comparison of gap thickness for these rods and their corresponding nodal LHGR are plotted in Figure 3-8.

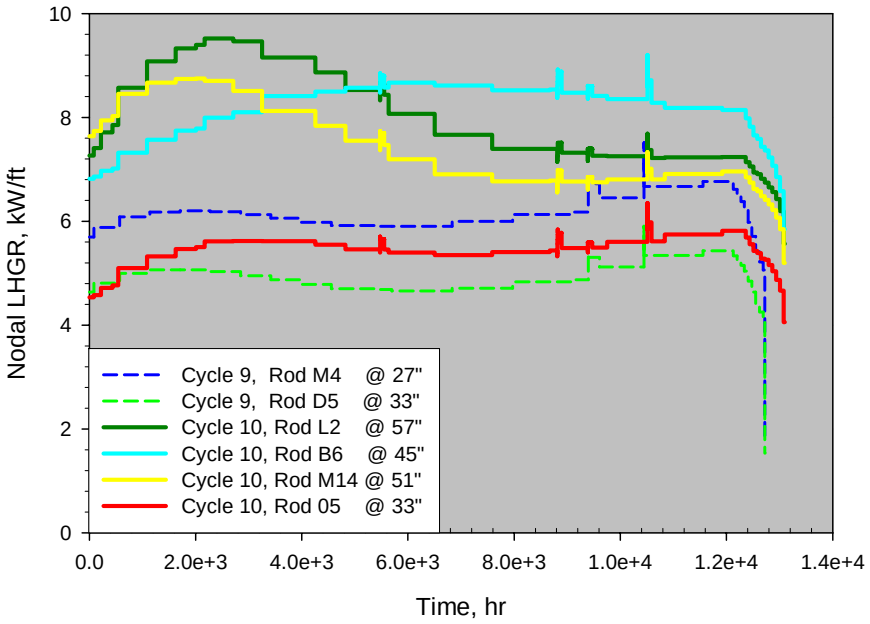

Figure 3-7
Nodal Power Corresponding to the Peak Stress Location during the Braidwood 1 Cycle-9 and 10 Base Irradiations

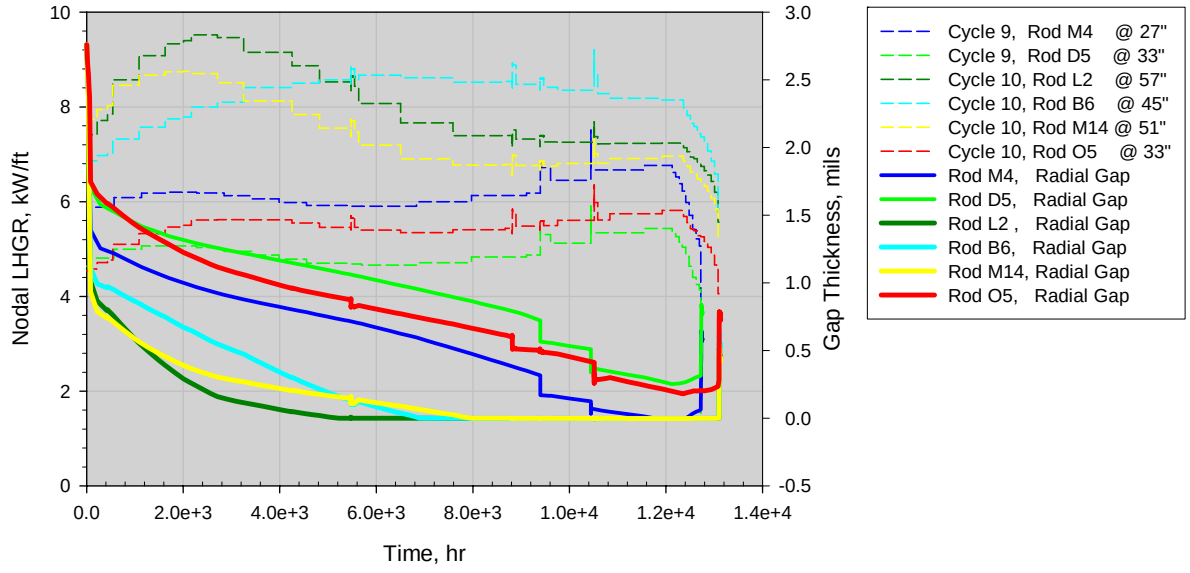

Figure 3-8
Fuel Rod Gap Thickness Corresponding to the Peak Stress Location during the Braidwood 1 Cycle-9 and 10 Base Irradiations

From the FALCON full length R-Z analysis of the Braidwood 1 Cycle 10 and 11 startup ramps, the maximum cladding hoop stress locations are determined for the failed and non-failed rods. For the O5 and D5 rods the maximum cladding hoop stress occurred in Element 141, which corresponds to the inner portion of the cladding at an axial elevation of approximately 33 inches. For the M4, M14, B6 and L2 rods, the peak cladding stress occurred at 27, 51, 45 and 57 inches from the bottom of the fuel column. The FALCON R-θ PCI local effects model was used to further evaluate the local stress concentration at these axial locations during the reactor startup ramps. The discontinuity of pellet cracks produces stress concentrations in the cladding. Figure 3-11 compares the peak stress in Element 73 (adjacent to the pellet crack) for the three Cycle 11 failed rods (B6, L2, and O5) and non-failed rod M14, with the two non-failed rods from the Cycle 10 startup. The M14, B6 and L2 rods have significantly higher stress than the non-failed rods from the Cycle 10 startup. The maximum local cladding hoop stress for the M4 rod is approximately 31 ksi, while the maximum stress in the M14 rod is about 49 ksi, about 1.6 times higher. The maximum cladding hoop stress for the B6 and L2 rods is about 40 and 45 ksi. The O5 rod with the nominal fuel rod dimensions shows relatively lower cladding stress (20 ksi), which is below FALCON's assumed value where PCI type cladding failure probability is considered to increase.

Several analyses were performed on the O5 rod to investigate the influence of a missing pellet surface or worst-case tolerance stack up on the PCI failure potential. The results of this sensitivity study are summarized in Table 3-6 and plotted in Figure 3-13 and Figure 3-14. Assuming a missing pellet surface was present in the O5 rod, the peak cladding stress at Element 73 increases from 20 ksi to almost 43 ksi and the CDI increases to 0.1. The worst-case tolerance stackup analysis results in an even higher calculated failure potential with peak cladding stress of 57 ksi and CDI of 21.6. For nominal fuel rod dimensions but with a slower helium release rate from the depletion of the ZrB_2, the cladding stress increases from 20 to 30 ksi, highlighting the important impact of rod internal pressure on the mechanical performance of a fuel rod.

Table 3-4
FALCON calculated Peak Cladding Stress and Cumulative Damage Index (CDI) for the Braidwood 1 Cycle 9 and 10 Fuel Rods

Assembly	Rod	Peak Stress Position (Inch)	Nodal Burnup (GWd/tU)	Cycle 9 Power After Coastdown (kW/ft)	Peak Nodal LHGR During Cycle 10 Startup (kW/ft)	Change in Power (kW/ft)	EOC 9 Peak Rod Internal Pressure (KSI)	Peak Stress (KSI)	CDI
L01S	M4	27	24.40	5.062	9.488	4.425	1.416	30.70	0.20
	D5	33	19.52	4.137	9.980	5.842	1.242	17.50	3.7E-3

Table 3-5
FALCON calculated Peak Cladding Stress and Cumulative Damage Index (CDI) for the Braidwood 1 Cycle 10 and 11 Fuel Rods

Assembly	Rod	Peak Stress Position (Inch)	Nodal Burnup (GWd/tU)	Cycle 10 Power After Coastdown (kW/ft)	Peak Nodal LHGR During Cycle 11 Startup (kW/ft)	Change in Power (kW/ft)	EOC10 Peak Rod Internal Pressure (KSI)	Peak Stress (KSI)	CDI
M16S	O5	33	22.09	4.662	9.126	**4.464**	1.617	20.42	8.4E-3
M36S	M14	51	30.44	5.846	8.794	2.947	1.814	49.41	6.61
M12S	B6	45	33.28	6.584	8.613	2.029	1.922	40.07	1.00
M19S	L2	57	32.98	6.197	8.050	1.852	1.856	44.87	2.48

Table 3-6
FALCON calculated Peak Cladding Stress and Cumulative Damage Index (CDI) for the O5 fuel rod during the Braidwood 1 Cycle 11 Startup

Assembly	Rod	Analysis Approach	Peak Stress Position (Inch)	Nodal Burnup (GWd/tU)	Change in Power (kW/ft)	EOC10 Peak Rod Internal Pressure (KSI)	Peak Stress (KSI)	CDI
M16S	O5	Baseline	33	22.09	4.464	1.617	20.42	8.4E-3
		Minimum Initial Gap				1.998	***56.96***	***21.60***
		Missing Pellet Surface				1.617	42.50	0.100
		50% He release				1.171	30.81	0.056

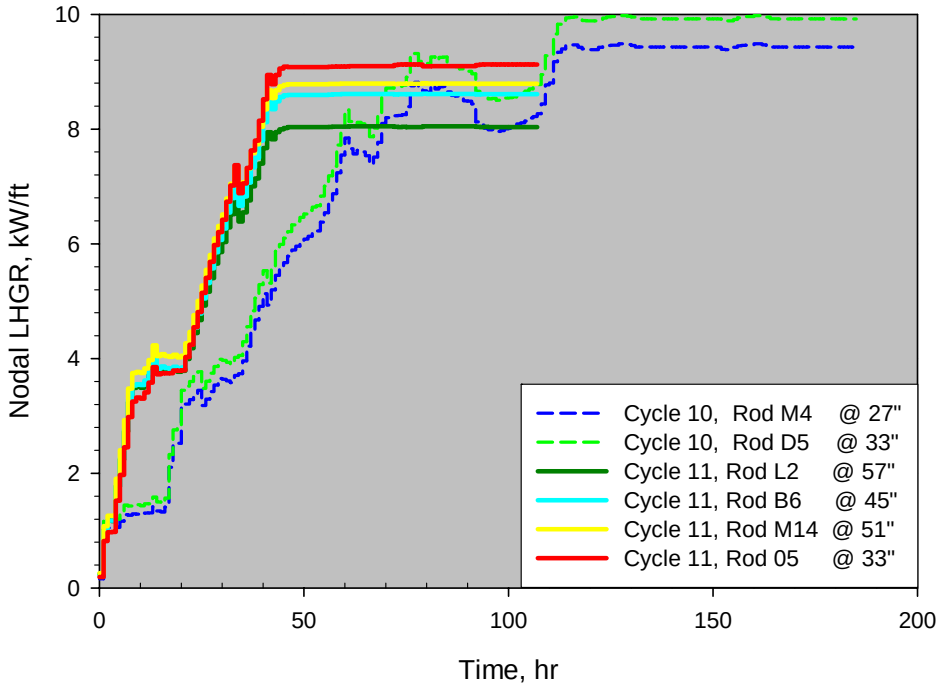

Figure 3-9
Nodal Power Corresponding to the Peak Stress Location during the Braidwood 1 Cycle-10 and 11 Startups

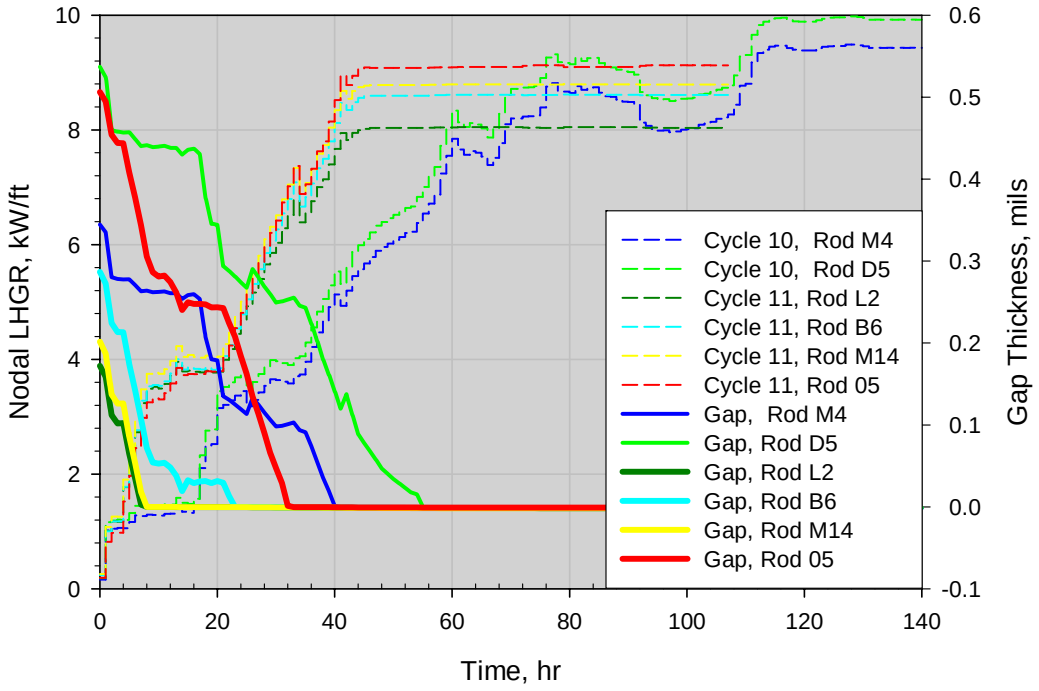

Figure 3-10
Fuel Rod Gap Thickness Corresponding to the Peak Stress Location during the Braidwood 1 Cycle-10 and 11 Startups

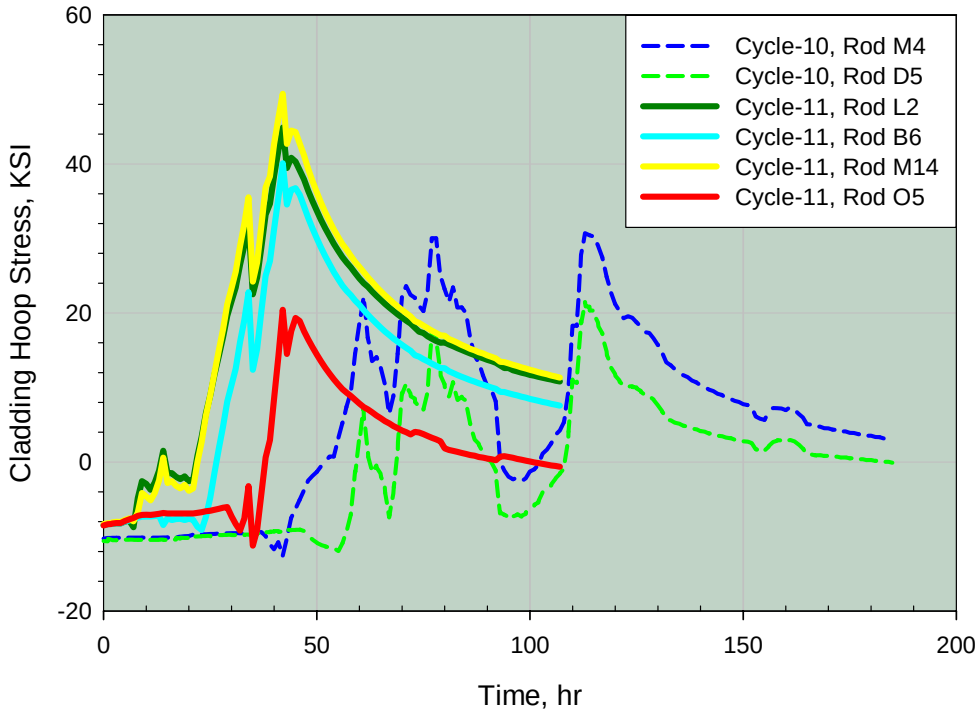

Figure 3-11
Comparison of the Cladding Hoop Stress during the Braidwood 1 Cycle 10 and 11 Startups

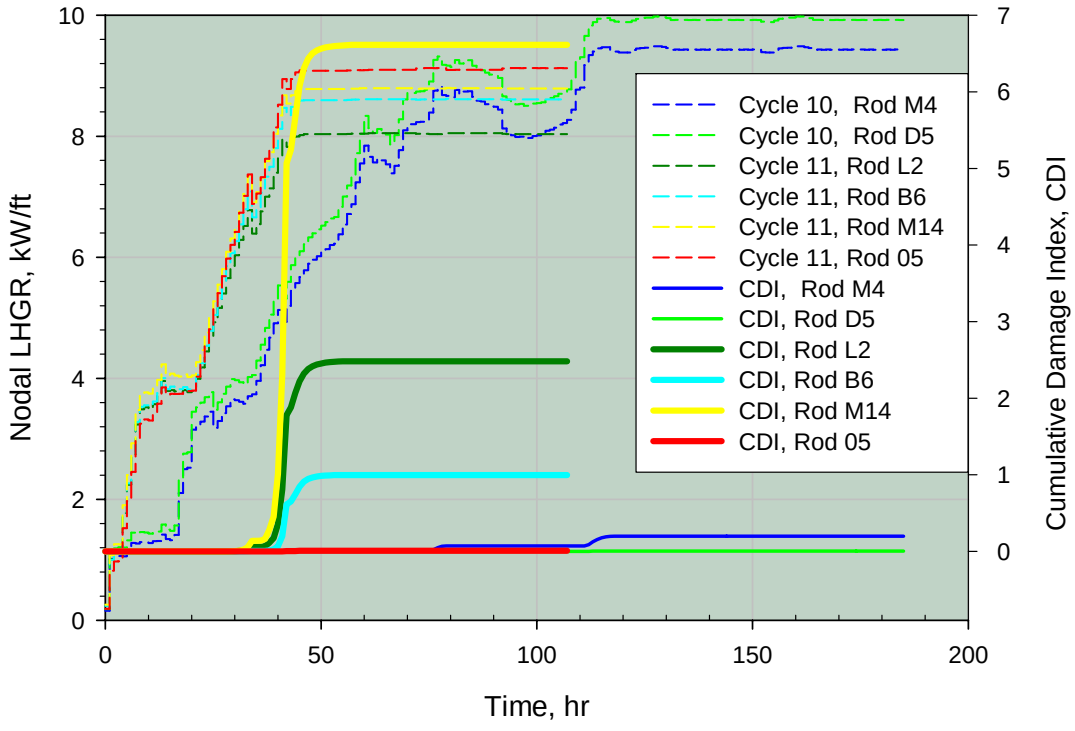

Figure 3-12
Comparison of the Cumulative Damage Index during the Braidwood 1 Cycle 10 and 11 Startups

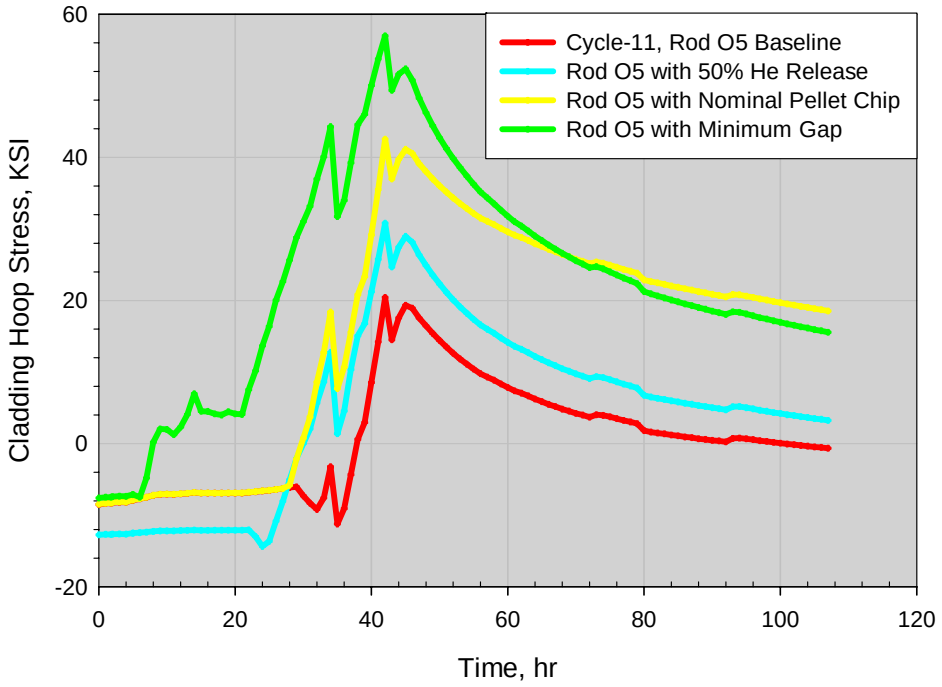

Figure 3-13
Cladding Hoop Stress for Different Stack-up and Operating Conditions for the O5 Rod

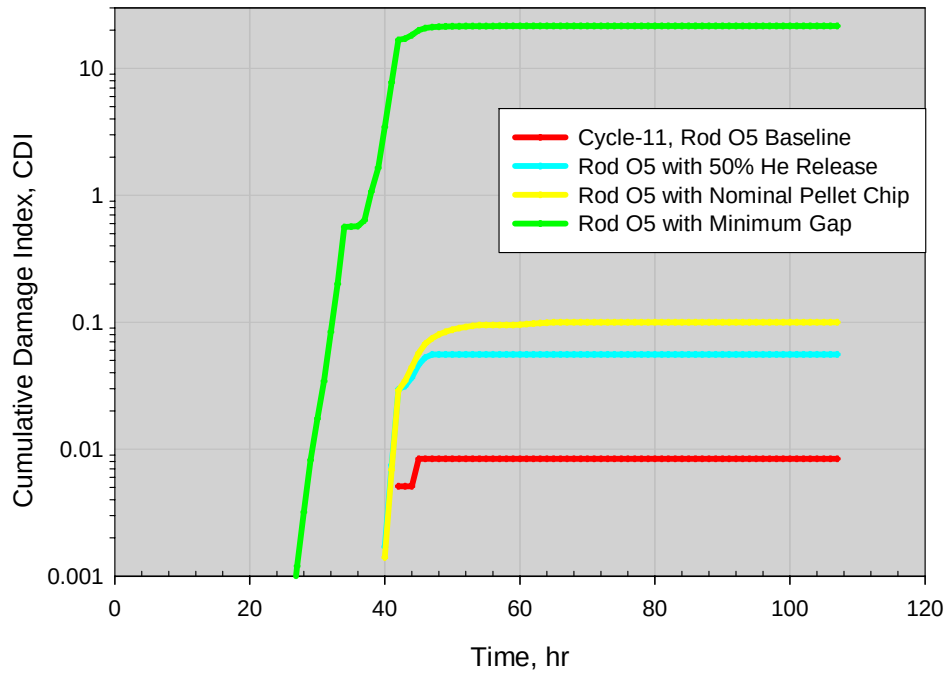

Figure 3-14
Cladding CDI for Different Stack-up and Operating Conditions for the O5 Rod

Contour plots of hoop stress in the fuel and cladding for the M14 rod during the Braidwood 1 Cycle 11 startup without missing pellet surface and with missing pellet surface, are shown in Figure 3-15 and Figure 3-16, respectively. The stress is most concentrated at the inner surface of the cladding adjacent to the pellet crack tip (upper edge of fuel elements as shown in Figure 2-2 and Figure 2-3). The missing pellet surface case shows the highest local stress, as expected. Table 3-7 summarizes the FALCON calculated peak cladding stress and CDI for the M14 rod for the baseline case and the missing pellet surface case. These analyses were performed assuming nominal pellet and cladding geometries and a missing pellet size as described in Table 3-3.

In order to investigate the effect of previous cycle power maneuvering such as MTC coefficient measurement, axial power swing due to xenon transition, coastdown, etc. on the PCI failure potential, several analyses was performed with rod M4 from assembly L01S. For these analyses the Braidwood 1 Cycle 9 base irradiation history was modified to remove the coastdown and MTC measurement event. The cladding hoop stress and CDI are plotted in Figure 3-17 through Figure 3-19 and summarized in Table 3-8. The peak cladding stress drops from 31 ksi to 24 ksi by removing the axial power swing due to the xenon transition. The coastdown and MTC events were found to have essentially no effect on the peak cladding stress, although the limiting rod was probably not chosen (for example, the pellet-clad gap in this rod was not closed until very near the end of Cycle 9).

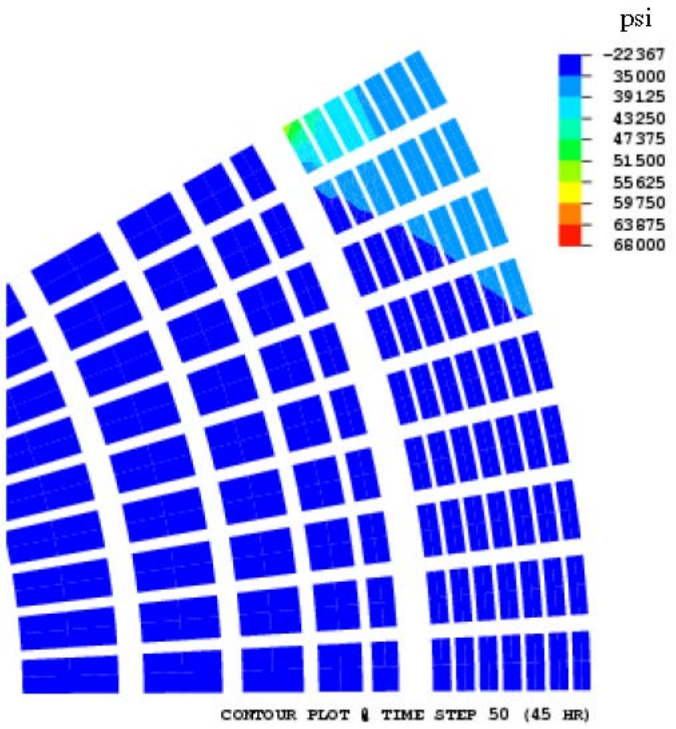

Figure 3-15
Hoop Stress Contour Plot for the M14 Rod during the Braidwood 1 Cycle 11 Startup (nominal pellet)

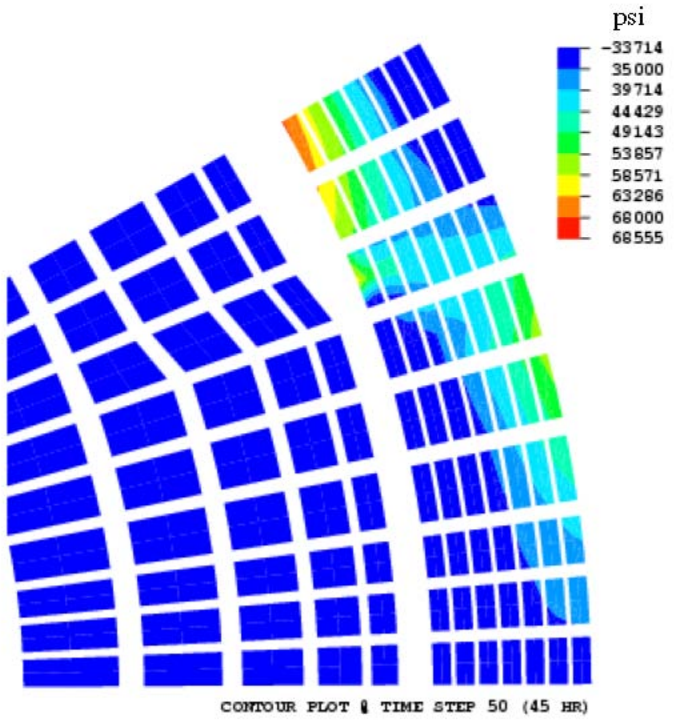

Figure 3-16
Hoop Stress Contour Plot for the M14 Rod with a Missing Pellet Surface during the Braidwood 1 Cycle 11 Startup (with missing pellet surface)

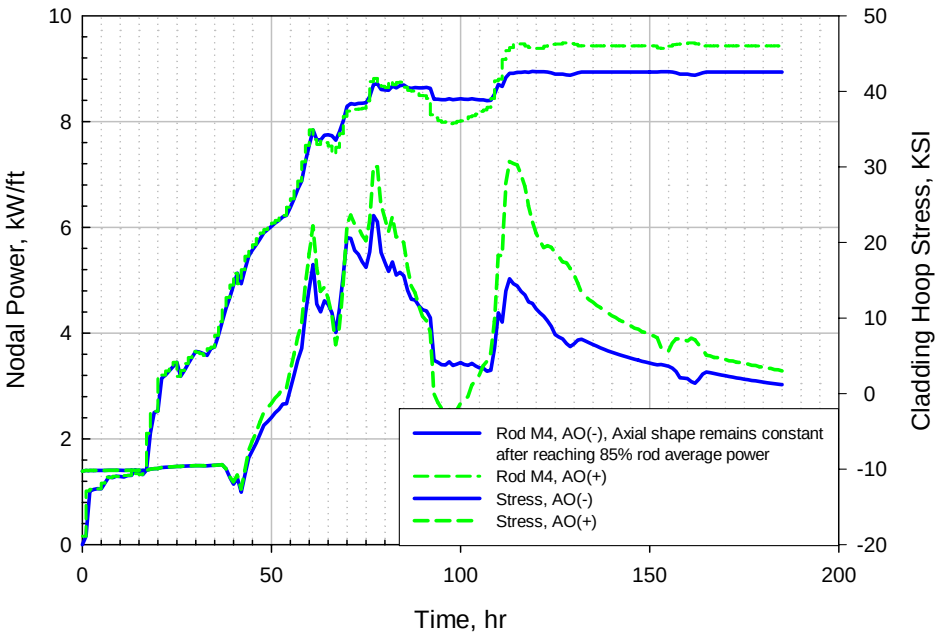

Figure 3-17
Axial Power Swing Effect during the Braidwood 1 Cycle 10 Startup

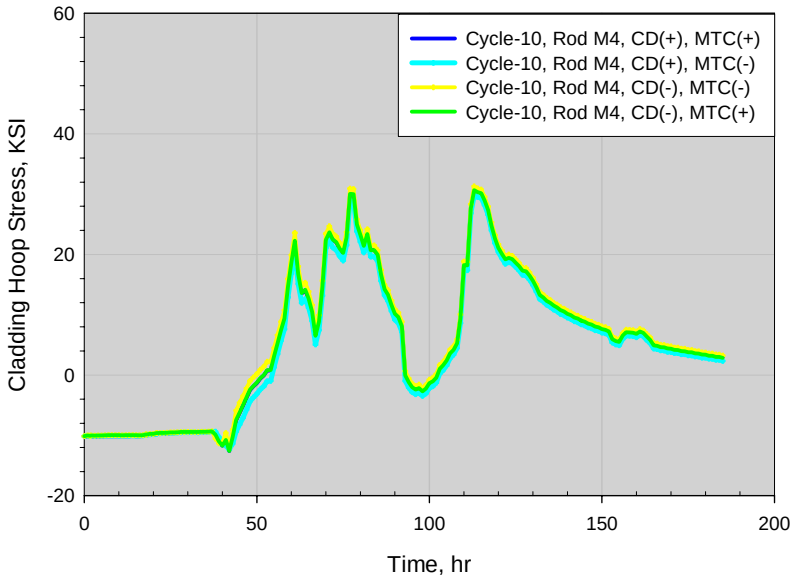

Figure 3-18
Rod Stress during the Braidwood 1 Cycle 10 Startup for the Cycle 9 Power Maneuvering

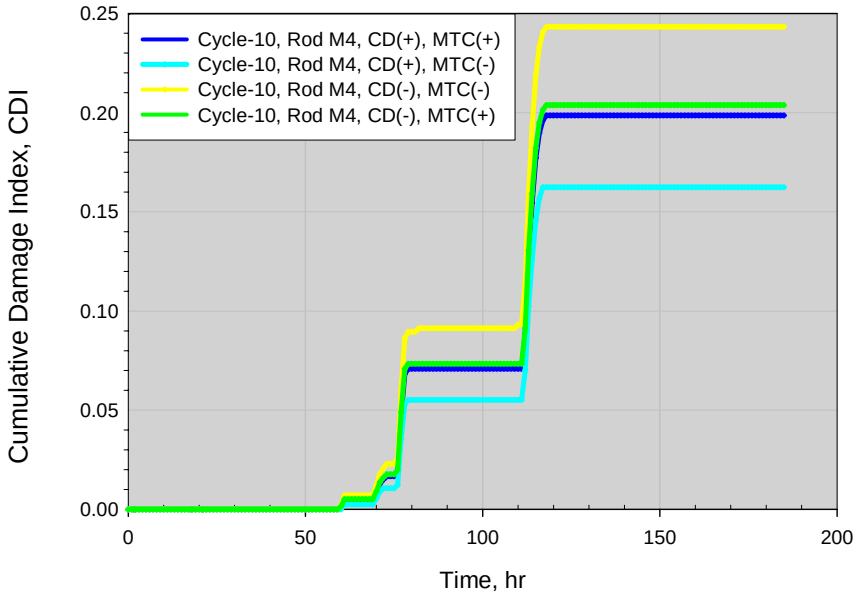

Figure 3-19
M4 Rod CDI during the Braidwood 1 Cycle 10 Startup for the Cycle 9 Power Maneuvering

Table 3-7
FALCON calculated Peak Cladding Stress and Cumulative Damage Index (CDI) for the M14 Fuel Rod during the Braidwood 1 Cycle 11 Startup

Assembly	Rod	Analysis Approach	Peak Stress Position (Inch)	Nodal Burnup (GWd/tU)	Change in Power (kW/ft)	EOC10 Peak Rod Internal Pressure (KSI)	Peak Stress (KSI)	CDI
M36S	M14	Baseline	51	30.44	2.947	1.814	49.41	6.61
		Missing Pellet Surface					***67.54***	***20.60***

Table 3-8
FALCON calculated Peak Cladding Stress and Cumulative Damage Index (CDI) for the M4 Fuel Rod during the Braidwood 1 Cycle 10 Startup

Assembly	Rod	Analysis Approach	Peak Stress Position (Inch)	Nodal Burnup (GWd/tU)	Change in Power (kW/ft)	EOC 9 Peak Rod Internal Pressure (KSI)	Peak Stress (KSI)	CDI
L01S	M4	CD (+), MTC (+), AO (+)	27	24.40	4.425	1.416	30.70	0.20
		CD (+), MTC (+), AO (-)					23.55	5.7E-3
		CD (+), MTC (-)**, AO (+)**					29.12	0.16
		CD (-)**, MTC (+), AO (+)**					30.35	0.202
		CD (-), MTC (-)**, AO (+)**					30.83	0.235

3.5 Byron 2 Cycle 13 Power Ascension Analysis Results

Three rods from Byron 2 Cycle 12 were selected for the Byron 2 Cycle 13 power ascension analysis. Rod C7 and D13 are from assembly T30E and represent higher burnup rods, Rod M14 is from assembly T13E and this rod has the largest power change of the selected rods. Figure 3-20 compares fuel rod nodal power histories for the selected Byron 2 Cycle 13 startup rods with Braidwood 1 Cycle-11 rods (failed rod B6 and non-failed rod M14). Both reactor startups have similar power ascension rate above 48% power. As a consequence, the Byron 2 Cycle 13 rods have peak cladding stresses projected to fall within the range of the Braidwood 1 Cycle 11 failed and non failed rods, which indicate a modification is necessary in the Byron 2 power ascension procedure to reduce the peak cladding hoop stress. The calculated peak cladding stress and cumulative damage index for the C7, D13 and M14 rods are plotted in Figure 3-21, Figure 3-22 and summarized in Table 3-9.

ANATECH worked with Exelon to modify the Byron 2 Cycle 13 power ascension procedure. Several options were considered and analyzed with FALCON. The options include hold times at 88%, 75% and 98% power that allow for stress relaxation and reduce the peak cladding stress and cumulative damage index. These cases assumed nominal pellet surfaces without missing pellet defects. Figure 3-23 shows three modified Byron 2 Cycle 13 power ascension profiles. Each of the profiles has different hold times and ramp rate combinations. The slower ramp rate profile reduces the peak cladding stress significantly at the same time results in the maximum loss of effective full power hours. The optimum power ascension profile will be a compromise between the lower peak cladding hoop stress produced by a lower ramp rate and less restrictive power ramp rate, which has a potential cost benefit for the operators.

The modified power ascension profile (1%/hr from 75 to 88% power and 0.5%/hr from 88 to 98% with a 5 hr hold at 88% power) reduces the peak cladding stress from 36 ksi to about 30 ksi for the D13 rod. This also reduces the Cumulative Damage Index from 1.09 to 0.2. Similar peak cladding stress and damage index values were observed for the M4 rod during the Braidwood 1 Cycle 10 startup. As the M4 rod survived at this stress level, this modified power ascension should provide significant margin for the PCI failure of the Byron 2 Cycle 13 rods.

Exelon requested ANATECH to reanalyze the Byron 2 Cycle 13 fuel rods with the modified power ascension profiles assuming a missing pellet surface is present in the fuel stack. The dimensions of the missing pellet surface used in the Byron 2 Cycle 13 analysis are those shown in Table 3-3. Again, working with Exelon, ANATECH introduced a modified power ascension profile with a further reduced ramp rate above 75% power. This modified power ascension profile has a ramp rate of 0.5%/hr from 75 to 98% power.

The results for the cladding hoop stress and CDI for all the three modified Byron 2 Cycle 13 power ascension profiles are presented in Figure 3-24 and Figure 3-25. The cladding hoop stress is above 40 ksi with the presence of a missing pellet surface for all the modified power ascension profiles. The case with a ramp rate of 0.5%/hr above 75% power has the lowest cladding stress and CDI of all the different power ascension profiles evaluated. For the nominal pellet and cladding geometries cases, the maximum cladding hoop stress drops to 23 ksi from 36 ksi for the 0.5%/hr ramp case, which is well below the maximum stress levels experienced in the

Braidwood 1 Cycle 10 successful startup, providing significant margin to PCI failure under these circumstances.

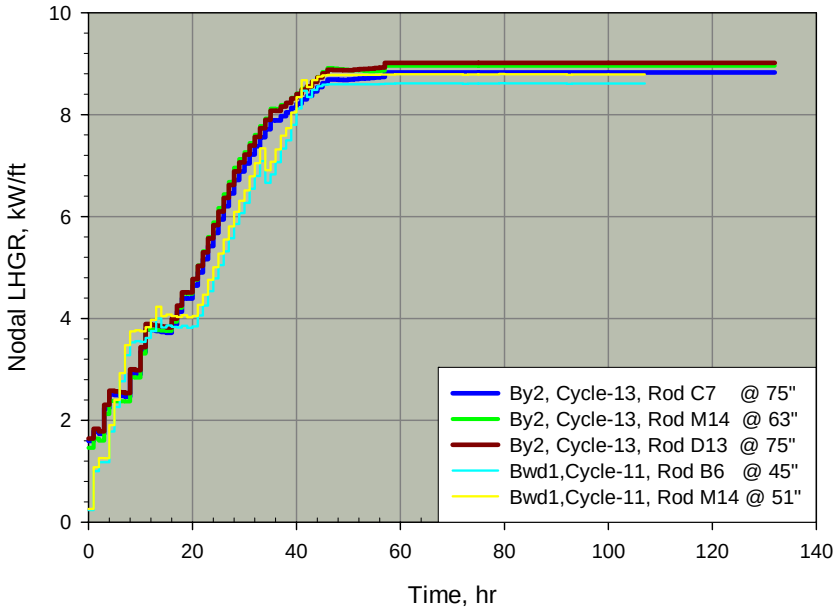

Figure 3-20
Fuel Rod Nodal Power for the Braidwood 1 Cycle 11 and Byron 2 Cycle 13 Startup

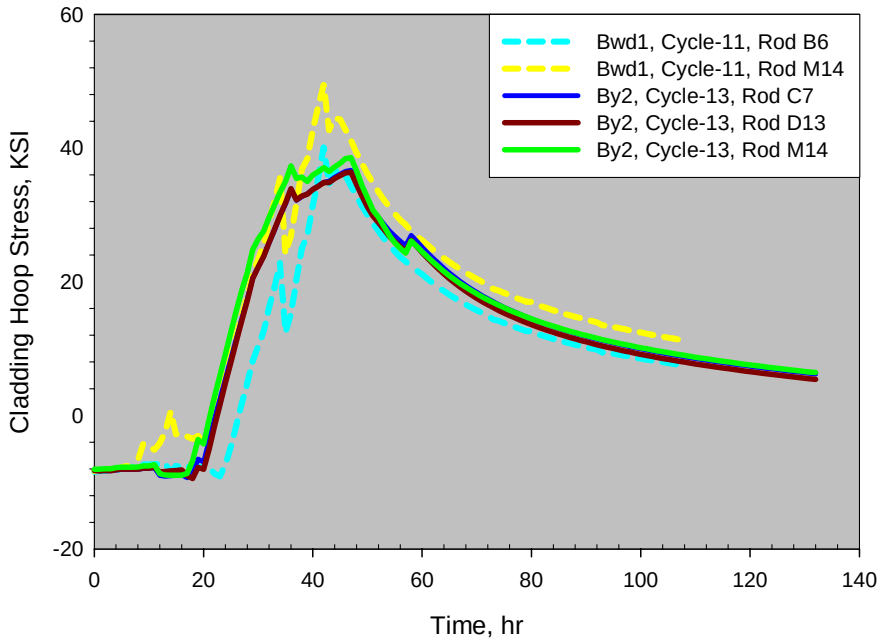

Figure 3-21
Cladding Hoop Stress during the Braidwood 1 C-11 and Byron 2 Cycle 13 Startup

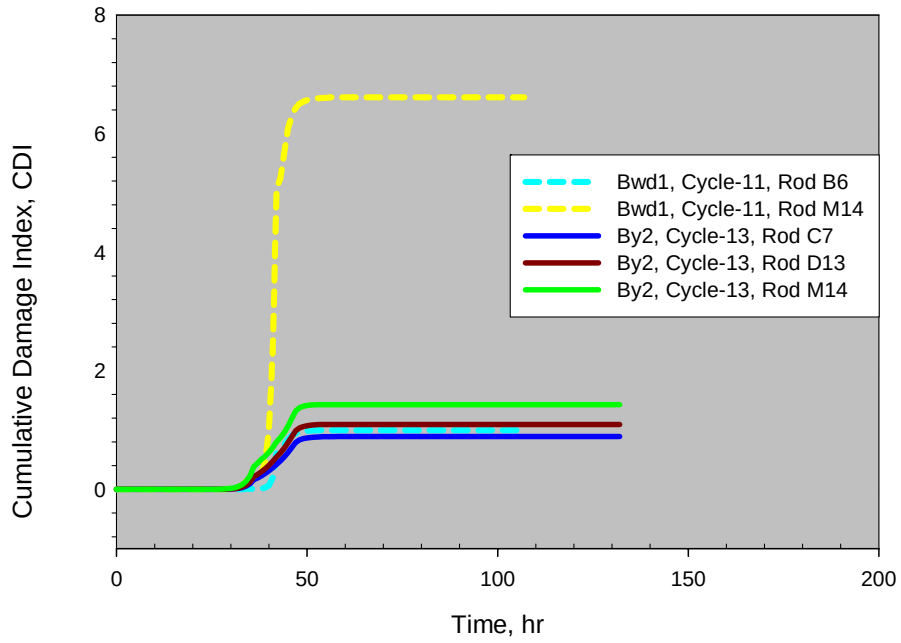

Figure 3-22
Cladding CDI during the Braidwood 1 Cycle 11 and Byron 2 Cycle 13 Startup

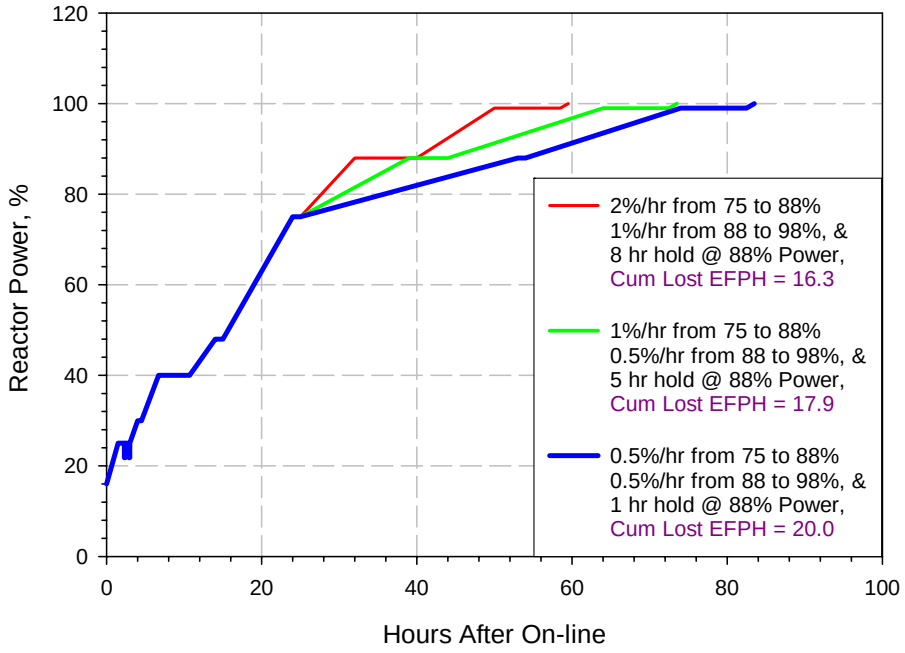

Figure 3-23
Byron 2 Cycle 13 Rod D13 Modified Power Ascension Profiles

Table 3-9
FALCON calculated Peak Cladding Stress and Cumulative Damage Index (CDI) for the Byron 2 Cycle 12 and 13 Fuel Rods (Baseline Cases; including coastdown)

Assembly	Rod	Peak Stress Position (Inch)	Nodal Burnup (GWd/tU)	Cycle 12 Power After Coastdown (kW/ft)	Peak Nodal LHGR During Cycle 13 Startup (kW/ft)	Change in Power (kW/ft)	Peak Rod Internal Pressure (KSI)	Peak Stress (KSI)	CDI
T30E	C7	75	31.62	7.111	8.828	1.716	1.916	36.67	0.89
	D13	75	31.88	7.283	9.015	1.731	1.943	36.38	1.09
T13E	M14	63	26.20	5.711	8.959	3.247	1.766	38.53	1.42

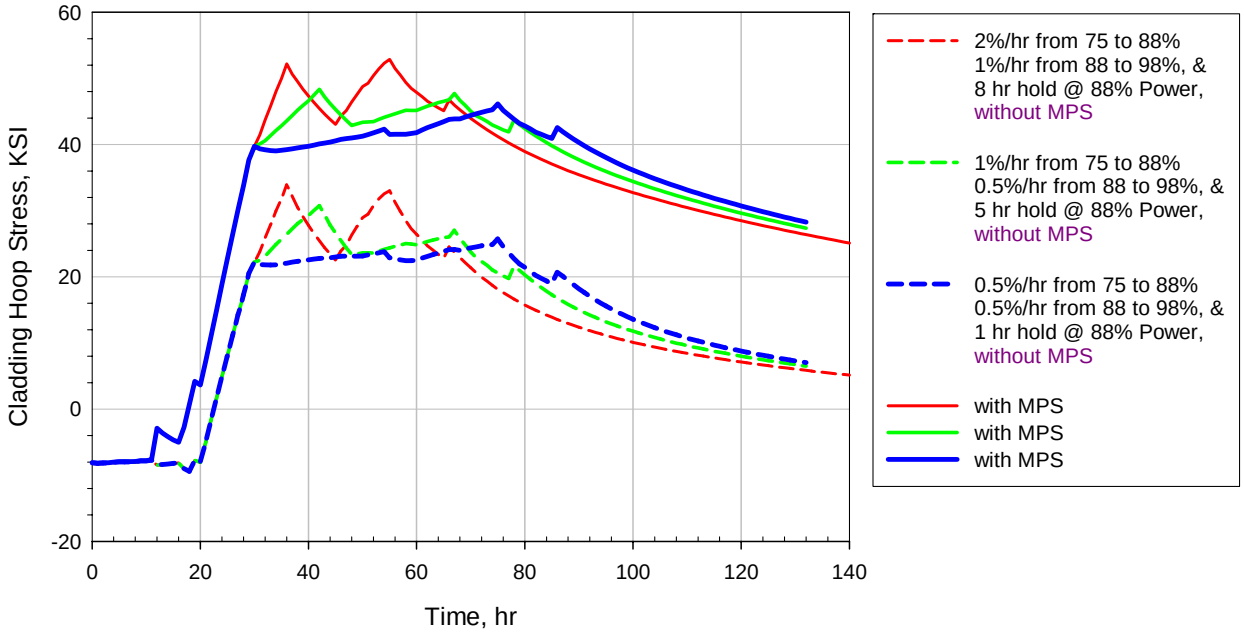

Figure 3-24
Byron 2 Cycle 13 Rod D13 Cladding Hoop Stress with and without Missing Pellet Surface (The ramp rate is ~5%/hr below 40% power and a ramp rate of 3%/hr is used between 40% and 75% reactor)

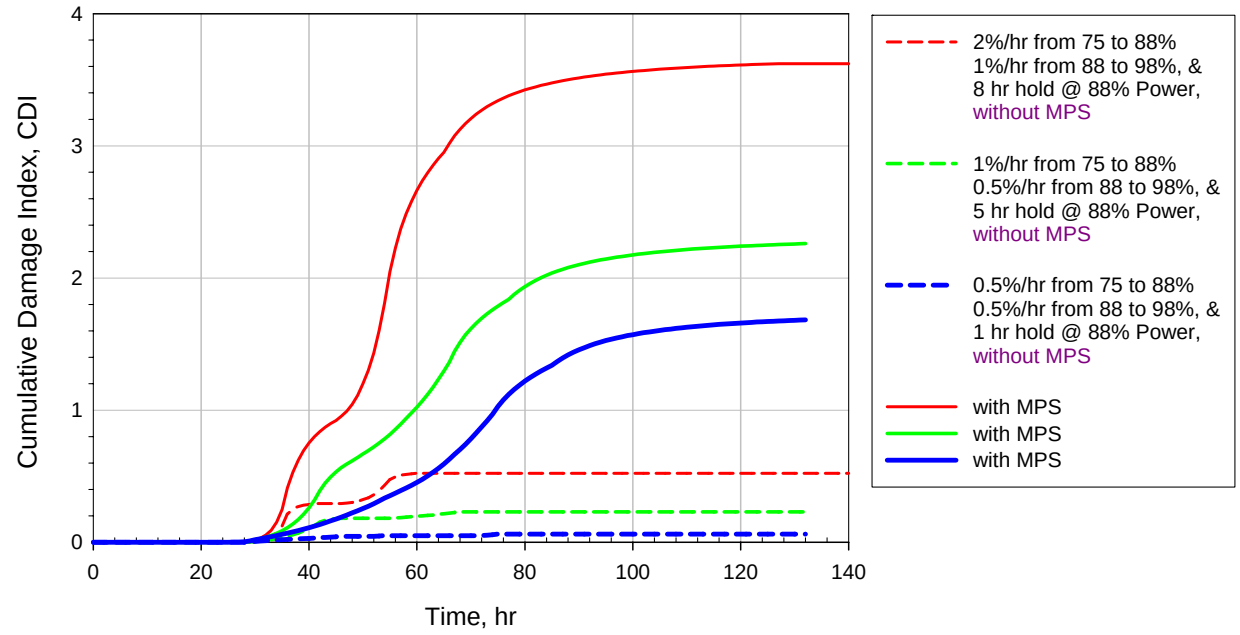

Figure 3-25
Byron 2 Cycle 13 Rod D13 CDI with and without Missing Pellet Surface

3.6 Byron 2 Cycle 13 Power Ascension Recommendations

Analysis of the initially planned startup profile for Byron 2 Cycle 13 indicated that the 3%/hr (40%-75%RP)-2%/hr (75%-90% RP)-1%/hr (90%-100% RP) strategy would not provide sufficient reduction of the cladding hoop stress and CDI to protect against PCI failure for the highest power/burnup rods, especially if defective pellets are present in the once-burned fuel. The FALCON analysis indicates that the following startup profile for Byron 2 Cycle 13, assuming the fuel has the same margin to PCI (or MPS-assisted PCI) as the fuel in Braidwood 1 Cycle 11, is recommended for Byron and Braidwood units to protect against the potential for PCI failures:

1. Unrestricted ramp rate below 40% of full power operation
2. 3%/hr reactor power increase rate between 40% and 75% of full power operation
3. 0.5%/hr reactor power increase rate between 75% and 100% of full power operation

In the event missing pellet surface (MPS) similar in size to that assumed in the FALCON calculation is identified as the failure mechanism in Braidwood 1 Cycle 11, the following relaxed reactor startup profile is recommended for Byron and Braidwood units to protect against the potential for PCI failure for cores without MPS:

1. Unrestricted ramp rate below 40% of full power operation
2. 3%/hr reactor power increase rate between 40% and 75% of full power operation
3. 1%/hr reactor power increase rate between 75% and 88% of full power operation
4. 5 hour hold period at 88% of full reactor power
5. 0.5%/hr reactor power increase rate between 88% and 100% of full power operation

4
BRAIDWOOD 2 CYCLE 10 FUEL FAILURE ANALYSIS

The Braidwood Unit 2 Cycle 10 fuel rod failure occurred following a return to full power after a short period of reduced power operation (load follow activity over a weekend). Poolside examinations performed after off-loading of the fuel assembly R36S confirmed a ~0.5" axial crack at the 21" elevation in the O5 rod. This assembly was first operated in Cycle 9 and irradiated for a second cycle during Cycle 10. At the time of the load follow power maneuver in cycle 10, the fuel rod average burnup was 43.7 GWd/tU and the nodal burnup at the 21" elevation was 47.9 GWd/tU. The power maneuver occurred approximately 392 days into Braidwood Unit 2 Cycle 10 and the fuel rod continued operation until the end of Cycle 10 at 530 days with a discharge rod average burnup of 54.2 GWd/tU.

As part of the Exelon root cause failure evaluation of the R36S-O5 rod, the FALCON fuel performance code was used to calculate the evolution of the cladding inner surface hoop stress and cumulative damage index during the maneuver in order to access the cladding failure potential by PCI. The objective of this analysis was to understand the role of power operation on cladding failure observed in rod O5. In addition, the insights gained from this analysis may provide guidance to the hot-cell examination planned for this rod.

The FALCON calculations were performed based on detailed fuel rod average and nodal power history data obtained from the ANC output provided by Westinghouse. The following summarizes 1) the steady state analysis performed to initialize the fuel rod conditions at the time of the power maneuver in Braidwood 2 Cycle 10, 2) the full-length R-Z analysis of the power ramp to 100% reactor power operation following the maneuver to identify the peak stress location, and 3) the PCI analysis of the power ramp to 100% reactor power following the load follow maneuver to calculate the local cladding stress and cumulative damage index (CDI) based on stress corrosion cracking.

4.1 Steady State Analysis of Rod O5 in Braidwood 2 Cycle 9 and Cycle 10

The steady state operation of the R36S-O5 rod during the Braidwood 2 Cycle 9 irradiation was calculated with FALCON using a full-length R-Z fuel rod model (see Figure 2-1). The FALCON calculation was restarted using the Cycle 10 power history up to the time of the first power reduction to calculate the fuel rod condition prior to the power ascension to full power. The Cycle 10 analysis also used the full-length (R-Z) model and calculated the cladding hoop stress distribution along the length of the fuel rod. The fuel rod average power history for the Cycle 9 and 10 irradiations are shown in Figure 4-1 and Figure 4-2, respectively. It should be noted that Braidwood Unit 2 was uprated about 5% approximately 200 days into the Cycle 9 as indicated in Figure 4-1.

As shown in Figure 4-2, the power maneuver at ~391 days after the start of Cycle 10 actually consisted of two reactor power decreases; a reduction in reactor power to ~69% and a second decrease in reactor power to ~75% about 5 days later. A close-up view of these power maneuvers is also shown in Figure 4-2.

The main purpose of the base irradiation analysis is to determine the initial conditions of fuel rod R36S-O5 at the time of the power maneuver suspected to have caused cladding failure in Cycle 10. The initial conditions of interest include the fuel rod internal pressure, the residual fuel-cladding gap, the cladding strain, and internal gas composition. During the Cycle 10 analysis, a detailed power history for the startup ramp was provided by Westinghouse from the ANC calculations. This detailed power history for the startup ramp was included in the FALCON calculation for Cycle 10 and the cladding hoop stresses during the startup ramp are compared to the power maneuver in the following section.

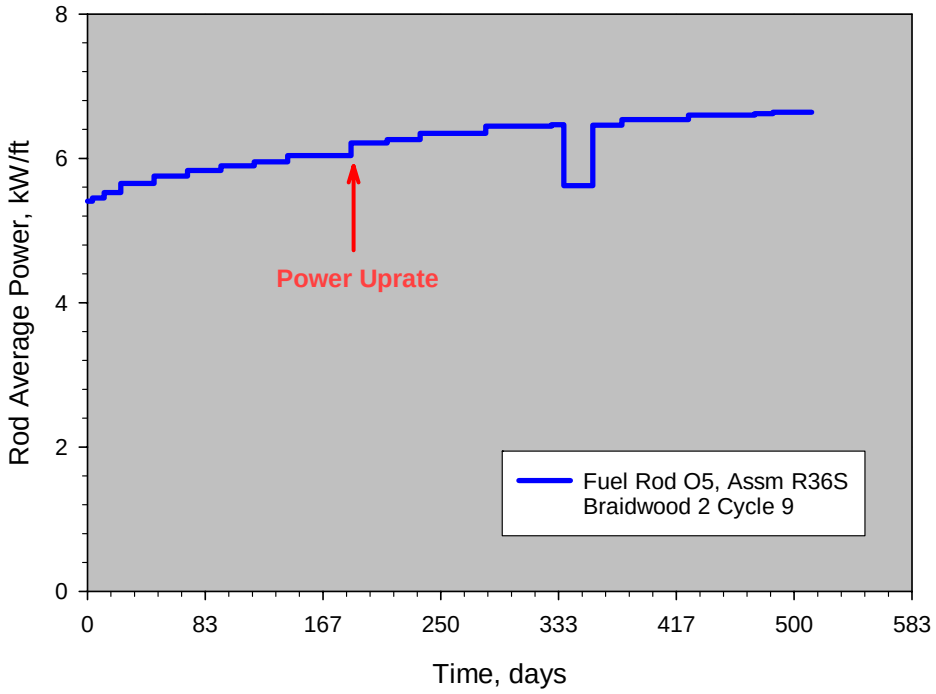

Figure 4-1
Braidwood 2 Cycle 9 Base Irradiation History for the O5 Rod

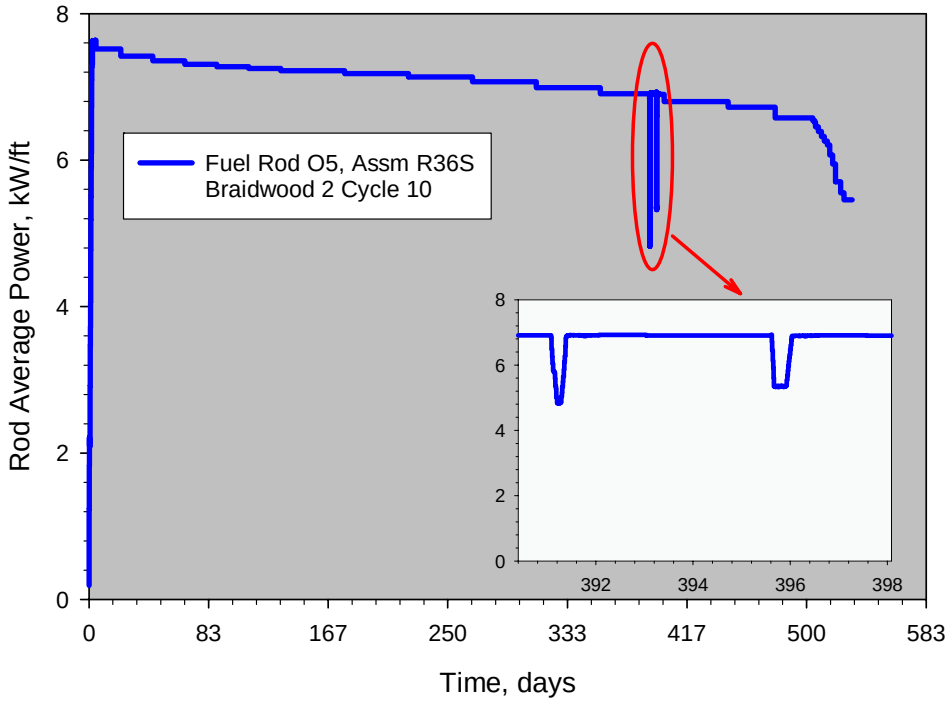

Figure 4-2
Braidwood 2 Cycle 10 Base Irradiation History for the O5 Rod

4.2 Power Ramp Analysis using Full-length (R-Z) and PCI (R-θ) Models

In the second step of the Braidwood Unit 2 Cycle 10 fuel rod analysis, a full-length R-Z calculation was performed for the power maneuvers associated with the return to full power. The purpose of this calculation was to identify the axial elevation of the maximum cladding hoop stress. In this way, the local fuel rod conditions, e.g., pellet-cladding gap at this axial elevation, can be used to initialize the local effects PCI model as described below. The results of the full-length R-Z model have also been used to compare the evolution of the cladding stress behavior during the startup of Cycle 10 with that experienced during the power maneuver later in the cycle. The power ramp calculation was restarted from the point in time of the reduced power operation just prior to the first return to full power.

The local effects PCI model in FALCON uses a R-θ geometry to analyze the evolution of the local cladding stress at an axial elevation in much greater detail than the R-Z model. The R-θ model (Figure 2-2 and Figure 2-3) is separate from the R-Z model, and whereas the power ramp analysis with the R-Z model can be initialized directly from the steady-state case output, the power ramp analyses using the R-θ model must be initialized manually using the output from the R-Z model. The information that must be input from the R-Z model includes the residual pellet-cladding gap, the rod internal pressure, and the cladding surface temperature. Furthermore, the analysis with the R-θ model must begin at zero power followed by a period of low power, e.g., at the base power of the ramp, in order to reach an equilibrium condition that closely matches the local fuel rod conditions namely, the temperature, stress and strain from the R-Z model.

4.3 Results of the Braidwood 2 Cycle 10 Fuel Rod Failure Analysis

As shown in Figure 5-2, the reactor power was decreased to 69% for a short time during the power maneuver. A second power reduction to 75% occurred about 5 days later. The time at reduced power was between 3 and 5 hours in each case. The reactor was returned to power full power at ~6% per hr following each power reduction. The nodal power history between the 10" and 33" elevations for Rod O5 is shown in Figure 4-3. Both of the power reductions are clearly evident in the figure. During the first return to power, a Xe-induced overpower condition develops in which the nodal power exceeds the power level prior to the maneuver by ~1.4 kW/ft. The return to full power combined with the Xe-induced overpower condition resulted in an overall power change of ~ 4.7 kW/ft between the 69% and the 100% reactor power statepoints. A similar response is observed 5 days later, with a slightly lower Xe-induced overpower condition. The Xe-induced overpower reaches a maximum about 5 hrs after reaching 100% power. During the return to 100% power, the largest impact of the Xe-induced overpower condition occurred at the 21" elevation. As shown in Figure 4-3, the Xe-induced power oscillations were terminated after the first major power overshoot in the fuel rod power history. This is expected to be conservative because the additional power oscillations are smaller in magnitude as compared to the first power peak.

Selected axial power shapes during the Braidwood 2 Cycle 10 are plotted in Figure 4-4 for the startup ramp, early steady-state power operation in Cycle 10, the first power reduction, and the first Xe-induced overpower condition. This plot illustrates the evolution of the axial power distribution for Rod O5 during the important events of Braidwood 2 Cycle 10. The two curves shown for the Cycle 10 startup ramp are at 92% and 100% reactor power and indicate that the peak power occurs near the 15" elevation. It should be noted that the power level at the 21" elevation reaches about 9.25 kW/ft. This bottom peaked power shape is partly due to Xe-induced axial effects as well as the core (reload) design. After ~90 days of irradiation, the strong bottom-peaking has burned out and the peak power location moves to the 50" elevation as shown by the steady state operation curves. After 391 days of irradiation, burnout of the fissile atoms in the middle of the rod leads to top and bottom power peaking and a more double-humped power shape. Just prior to the first power reduction, the peak power location is at the 117" elevation as shown in Figure 4-4. During the first power reduction, the overall fuel rod power decreases as shown in Figure 4-4, with a more prominent effect in the lower portion of the fuel rod. At the completion of the power decrease, the local power was reduced ~46% at the 21" elevation. At the completion of the return to power, the axial power shape is very similar to that just prior to the power reduction. As mentioned previously, a Xe-induced overpower condition occurs in the lower portion of the fuel rod once 100% reactor power condition is reached. The local power at the 21" elevation exceeds the pre-transient power level by ~1.4 kW/ft about 5 hrs after the return to full power. The axial power variation during the 5 hrs following the return to full power is shown in Figure 4-4. The maximum power reached during the first Xe-induced overpower condition is ~8.7 kW/ft, which is slightly below that reached during the startup of Cycle 10.

The calculated pellet-cladding gap at the 21" elevation is shown in Figure 4-5 for Cycle 9 and Figure 4-6 for Cycle 10. The FALCON results find that the local pellet-cladding gap closed about 370 days into the Cycle 9 irradiation, and due to the EOC depressurization and reactor shutdown, the gap opens up at the end of Cycle 9. During the startup of Cycle 10, the pellet-cladding gap is calculated to close and remains closed during the Braidwood 2 Cycle 10 irradiation until the shutdown at EOC. The power reduction during the maneuver is not

sufficient to reopen the pellet-cladding gap. However, a reduction in the pellet-cladding contact force is calculated to occur.

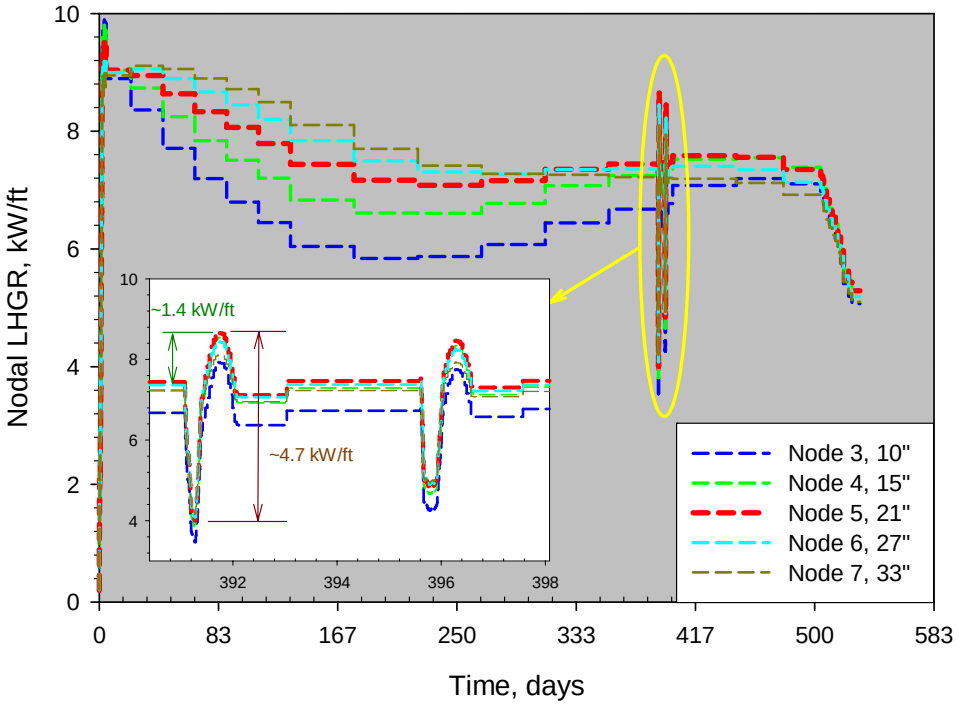

Figure 4-3
Braidwood 2 Cycle 10 Nodal Power Histories for the R36S O5 Rod

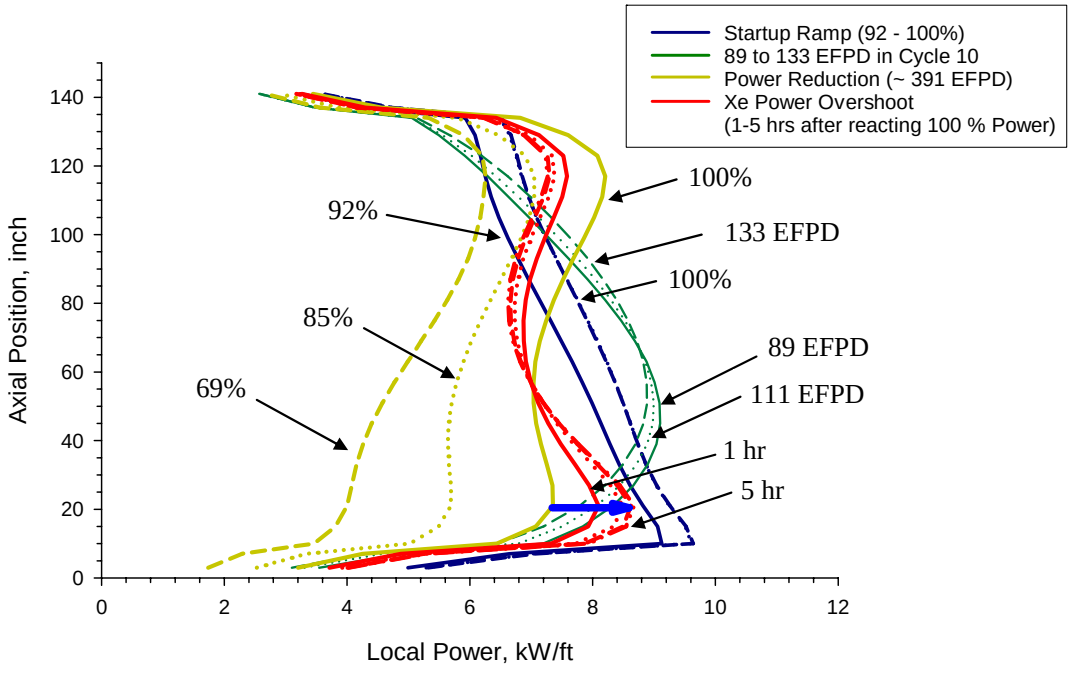

Figure 4-4
Braidwood 2 Cycle 10 Local Powers as a function of Axial Positions for the R36S O5 Rod

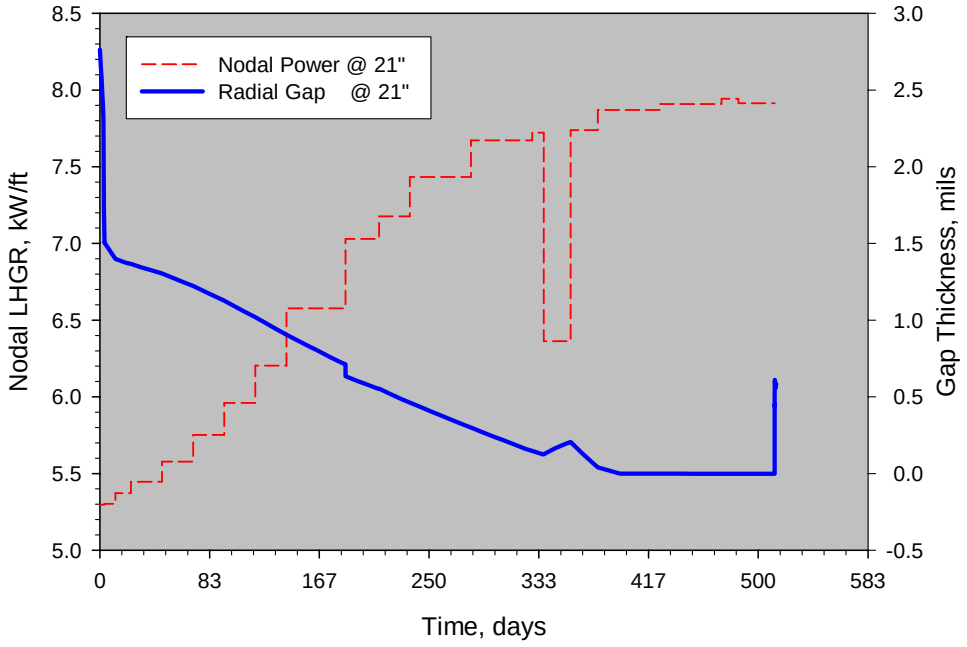

Figure 4-5
O5 Rod Radial Gap during the Braidwood 2 Cycle 9 Irradiation

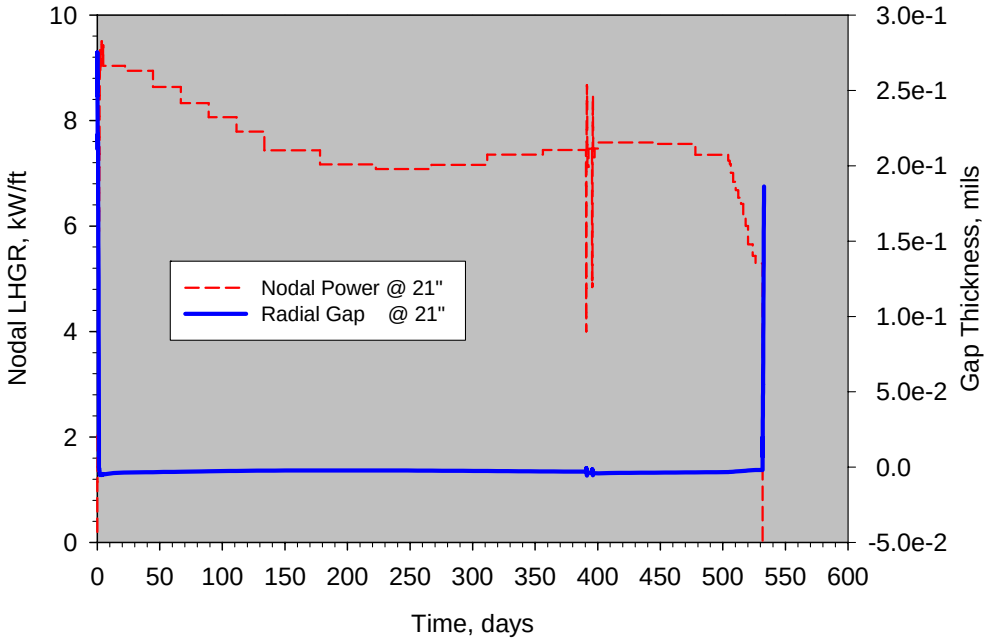

Figure 4-6
O5 Rod Radial Gap during the Braidwood 2 Cycle 10 Irradiation

The cladding hoop stress calculated during the Braidwood 2 Cycle 10 irradiation using the FALCON full-length R-Z model is shown in Figure 4-7 for elements ranging between the 16" elevation (Element 136) to the 40" elevation (Element 144). Element 138 corresponds to the 21" elevation. During the startup of Cycle 10, the cladding stress reaches a maximum in the region between the 30" and 40" elevations due to a combination of the axial distributions of the power, burnup, and residual pellet-cladding gap thickness. A maximum cladding hoop stress of ~28 ksi is calculated by FALCON to occur in this region following the Cycle 10 startup. The cladding hoop stresses introduced during the Cycle 10 startup decrease during the early part of the cycle irradiation due to creep-induced stress relaxation in both the pellet and the cladding. As mentioned in Section 3, the ZIRLO creep rate is modeled in these FALCON calculations to be less than the Zircaloy-4 creep rate. This slows the rate of creep-induced stress relaxation during the early part of the cycle. During the return to power following the maneuver, the maximum cladding hoop stress occurred at an axial elevation of approximately 21 inches from the bottom of the fuel as shown in Figure 4-7. Although this region had comparatively lower stress during the Cycle 10 startup, the tight pellet-cladding gap as well as larger power change at this axial elevation results in higher cladding stress during the power maneuvering events.

Figure 4-8 contains selected axial distributions of the cladding hoop stress during the Braidwood 2 Cycle 10 startup, the steady-state operation of Cycle 10, and the return to power. These results highlight the local increase in cladding hoop stress at the lower part of the fuel rod. At the time of failure this twice-burnt fuel had an average burnup of 43.7 GWd/tU and a nodal burnup of 47 GWd/tU at the 21" elevation. The axial distribution of burnup at the time of cladding failure and at the end of Cycle 10 is shown in Figure 4-9 for rod R36S-O5.

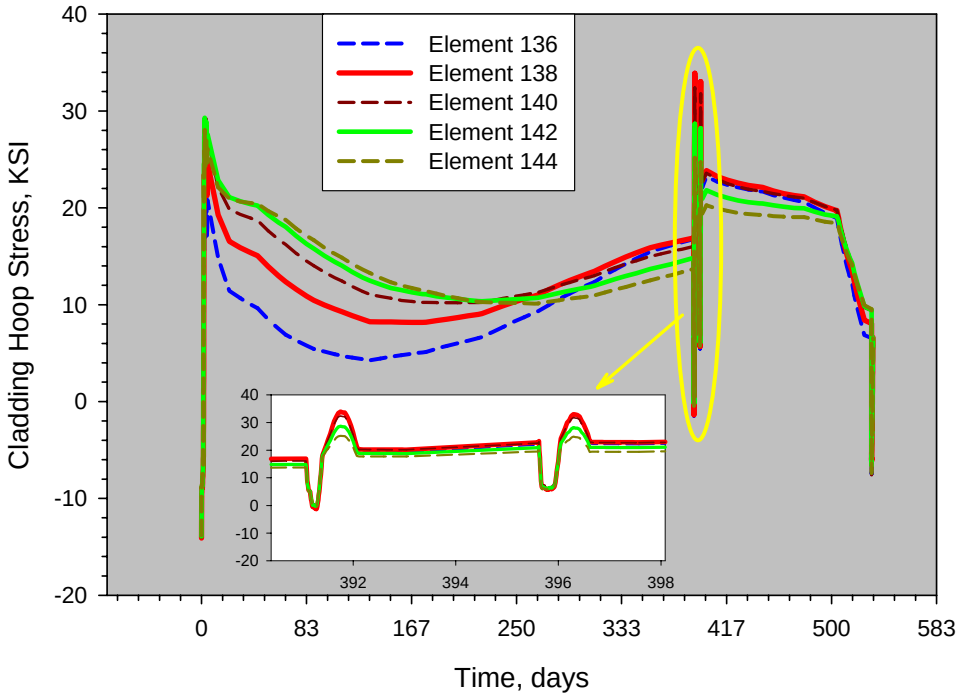

Figure 4-7
Cladding Hoop Stress for the O5 Rod during the Braidwood 2 Cycle 10 Irradiation

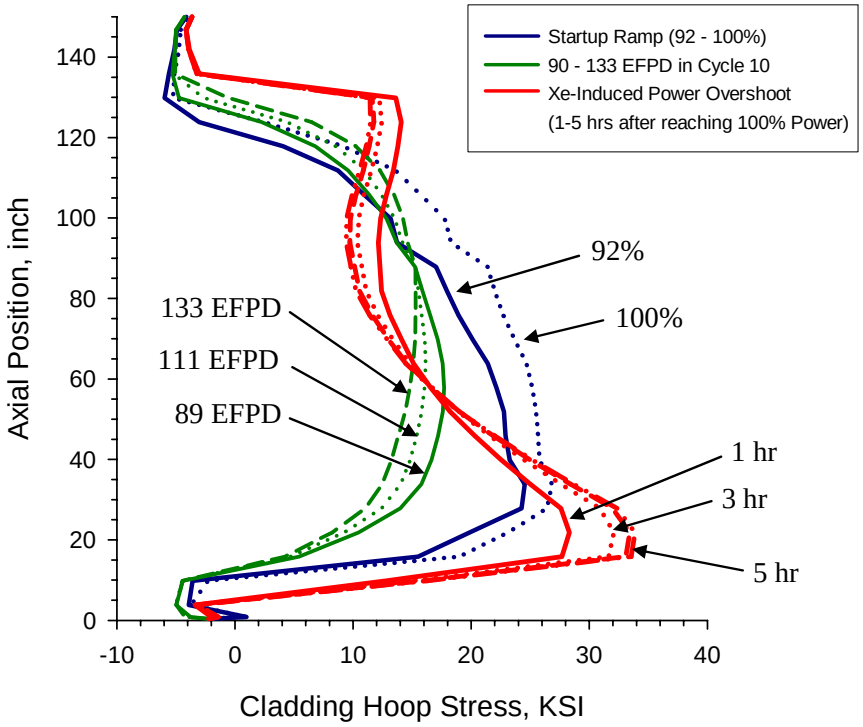

Figure 4-8
Cladding Hoop Stress as a function of Axial Position for the O5 Rod during the Braidwood 2 Cycle 10 Irradiation

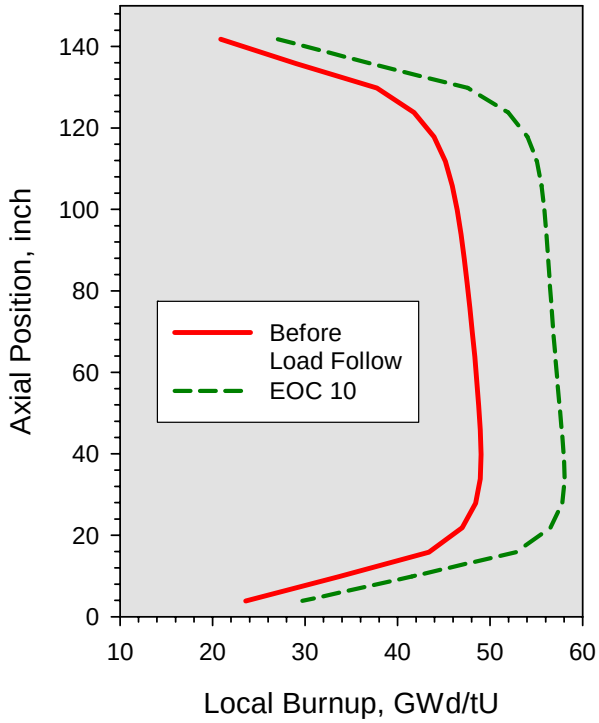

Figure 4-9
Axial Burnup Distribution for the O5 Rod during the Braidwood 2 Cycle 10 Irradiation

The FALCON R-θ PCI local effects model was used to further evaluate the localized cladding inner surface hoop stress at the 21" axial elevation where the peak power and cladding stress is calculated to occur in the R-Z model during the power maneuver. This model was initialized using the fuel rod conditions such as pellet-cladding gap thickness, internal pressure, gas composition, burnup, T/H conditions, etc, from the full-length steady state analysis of the Braidwood 2 Cycle 10 irradiation. The FALCON R-Z analysis of Cycle 10 was terminated just prior to the return to 100% power following the first power reduction at ~391 days. Because the R-θ model in FALCON must be started at zero power, the initialization phase includes a slow ramp from zero power to the base power level, with a hold of 24 hrs at the base power level, before the actual ascension to the full power. This is required to allow FALCON to reach an equilibrium state that is equivalent to the conditions calculated by the R-Z model. The calculated cladding inner surface hoop stress and the nodal linear heat generation rate are plotted in Figure 4-10 for the R36S-O5 rod. A similar plot for the cumulative damage index (CDI) is shown in Figure 4-11. Cladding inner element 73, which is adjacent to the pellet crack in the R-θ model, reaches a maximum stress of about 52 ksi and a cumulative damage index (CDI) of 7.7 following the two power maneuvers.

The FALCON calculated maximum inner surface cladding hoop stress for Rod O5 in assembly R36S is certainly above the stress threshold noted in Section 2.3 where the stress corrosion cracking (SCC) type cladding failure is possible in the presence of fission products. This fact is reflected in the high value of the CDI calculated for this rod. Moreover, the axial elevation of the peak cladding stress calculated by FALCON (21 inch from the bottom of the fuel) is consistent with a failure location observed in the post irradiation examinations. For reference, the calculated CDI for this rod is higher than the Braidwood 1 Cycle 11 failed rods. Moreover, the presence of a pellet defect in the peak cladding stress location would further increase the cladding hoop stress and CDI.

In summary, the FALCON calculations demonstrate that the failure of rod R36S-O5 is most likely related to the increased cladding hoop stresses during the return to full power following the power reduction in the later part of Braidwood 2 Cycle 10. The local power peaking resulting from the Xe-induced power overshoot results in the peak stress coinciding with the axial elevation where the suspected primary cladding failure site has been observed. The presence of pellet defects would further increase the peak cladding stresses.

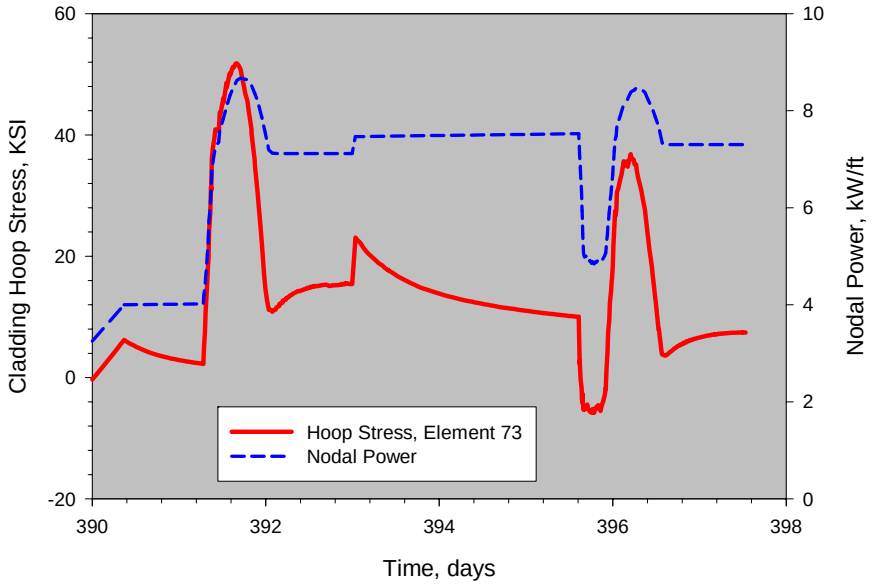

Figure 4-10
Cladding Maximum Hoop Stress (R-θ model) during the Braidwood 2 EOC 10 Power Maneuver

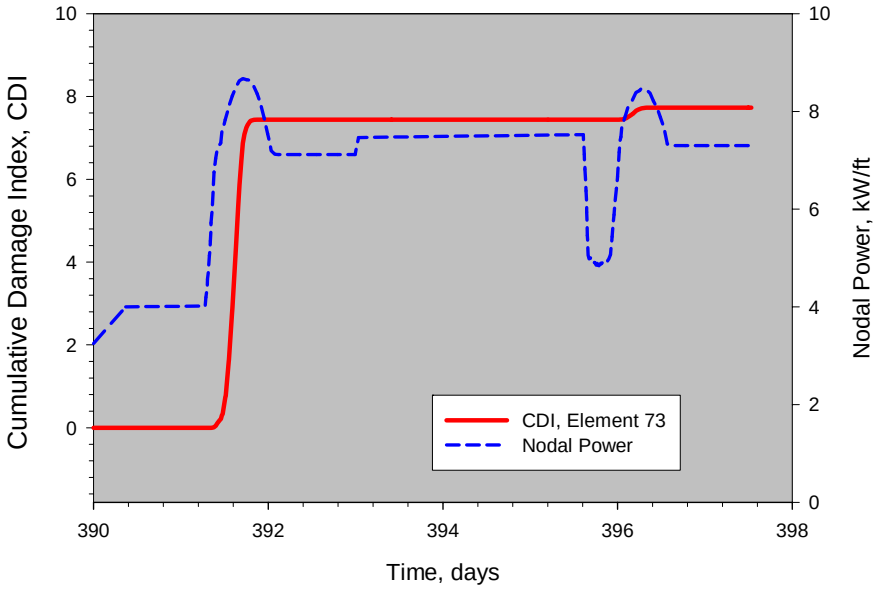

Figure 4-11
Cumulative Damage Index (R-θ model) during the Braidwood 2 EOC 10 Power Maneuver

5
SUMMARY AND CONCLUSION

The present report summarizes the FALCON analysis results for two (2) rods from the Braidwood 1 Cycle 10 startup, three (3) failed rods and a non-failed rod from the Braidwood 1 Cycle 11 startup, one (1) failed rod from the Braidwood 2 Cycle 10 mid-cycle power maneuver, and three (3) rods from the Byron 2 Cycle 13 startup. The objectives of these analysis were to 1) evaluate the cladding stress conditions at the suspected time of cladding failure to assess the potential role of PCI in the failure process and 2) provide reactor startup ramp recommendations for Byron 2 Cycle 13 to minimize the potential for PCI-type cladding failure.

The cladding hoop stress and the Cumulative Damage Index (CDI) results from the Braidwood 1 Cycle 10 fuel rods were used as a baseline for a successful reactor startup. The FALCON analysis demonstrated that both cladding hoop stress and cumulative damage index increased significantly during the startup ramp for once-burned fuel between the Braidwood 1 Cycle 10 startup and the Braidwood 1 Cycle 11 startup. The increase in the mechanical loading on the cladding caused by pellet-cladding mechanical interaction is a result of the faster startup ramp rate and axial flux deviation swing in the Braidwood 1 Cycle 11 power ascension as compared to the Cycle 10 startup in combination with the high powers levels used in these core designs. Furthermore, the increased fuel duty, which when combined with the occurrence of unfavorable fuel rod geometry variations within the tolerance specifications or deviations in the performance assumptions used in the fuel rod design, has brought into consideration the potential for PCI failure based on the assumed FALCON threshold.

For the Braidwood 2 Cycle 10 failure during the mid-cycle power maneuver, FALCON calculates a higher cladding stress and cumulative damage index than the Braidwood 1 Cycle 11 failed rods for the nominal pellet geometry. The higher burnup and tightly closed pellet-cladding gap for this twice burned fuel rod as well as a high local power change (~1.4 kW/ft) due to a Xe-induced power overshoot condition resulted in the increased cladding stress and the increased potential of PCI-type cladding failure.

BWR experience, supported by analytical validation, has demonstrated that a missing pellet surface increases the likelihood of a cladding failure under PCI conditions. This is consistent with the present FALCON analyses, which show that the presence of a missing pellet surface accentuates cladding stress during power ascension.

The statistical nature of PCI failures, which occur at a tiny fraction of fuel rods, cannot be entirely explained considering nominal fuel rod design or normal operational conditions. The small failure frequency attributed to PCI is the consequence of the stochastic process of worst-case combination of tolerances for manufacturing and/or operational variables that affect the evolution of cladding stresses. These variables include: variations in pellet and cladding dimensions, pellet missing surfaces as already mentioned, non-concentric pellet axial stacking,

uncertainties in fuel relocation and cladding creep-down during earlier cycles, fuel cracking patterns and their coincidence with pellet missing surfaces, uncertainties in power history and axial profile, rod internal pressure, uncertainties in power ramp rates, and other less important variables. Factors related to the transport of chemical species responsible for PCI to the cladding surface, although not part of this evaluation, are also important and likely add to the stochastic nature of this mechanism. Considering all of these variables, individually or combined, it is important to emphasize that the objective of a PCI failure analysis, as the one described in this report, is not to explain why certain rods fail while a thousand others subjected to similar, or even more aggressive power duty, do not, but rather to determine a safe power ascension procedure in the event that conditions conducive to PCI may develop. Thus, regardless of whether PCI failures are power-operation related or fuel manufacturing related, power-maneuvering restrictions, such as those as recommended in this report, can reduce the risk of cladding failure.

Several possible startup profiles for the Byron 2 Cycle 13 startup have been analyzed to evaluate the effectiveness to reduce the PCI type cladding failure potential. It is found that a power ascension profile with an unrestricted ramp rate below 40% power and 3%/hr ramp rate from 40% to 75% and 1.0%/hr ramp rate between 75% and 88%, 0.5%/hr from 88 to 100% power with a 5 hr hold at 88% power will protect the fuel rods against PCI type failures. For the case of a missing pellet surface, this analysis recommends a slower startup ramp, which consists of unrestricted ramp rate below 40% power and 3%/hr ramp rate from 40% to 75% and 0.5%/hr ramp rate between 75% and 100% power. With the hold times assumed in Figure 4-17, the additional loss of EFPH between the originally propose strategy and the most conservative strategy is 3.7 hours.

The potential for PCI failure was shown to be insensitive to the moderator temperature coefficient power maneuver, the reactor coastdown at the end of the cycle, and the depressurization/temperature history, although the limiting rod was likely not considered. In contrast, local axial power increases occurring in conjunction with non-equilibrium Xe-induced reactivity variations may produce local ramp-rates that exceed the rate restrictions, and therefore minimizing the axial power variations (AO) during the reactor startup decreases the potential for PCI failure.

6
REFERENCES

1. Fuel Analysis and Licensing Code: FALCON MOD01: Volume 1: Theoretical and Numerical Bases, EPRI, Palo Alto, CA: 2004. 1011307.
2. G. Sabol et al, "In-Reactor Corrosion Performance of ZIRLO and Zircaloy-4," *Zirconium in the nuclear Industry: Tenth Symposium ASTM STP 1245*, 1994, pp. 724-744.
3. Westinghouse Memo, " Generic Data Requirements for PCI Analysis," PPE-05-159, July 7, 2005
4. Y. R. Rashid, A. J. Zangari and C. L. Lin, "Modelling of PCI Under Steady State and Transient Operating Conditions," Water Reactor Fuel Element Computer Modelling in Steady State, Transient and Accident Conditions, Proceedings of a Technical Committee lMeeting, IAEA-TC-659/2.3, IAEA, 1989, pp. 91-101.
5. Westinghouse Memo, "Rod Power history Data for transmittal to ANATECH," PCT-05-542, July 1, 2005
6. Westinghouse Memo, "ANC Identification of Failed Rods in Braidwood Unit 1," PPT-05-54, July 5, 2005
7. Westinghouse Memo, "Rod Power history Data for transmittal to ANATECH," PCT-05-556, July 14, 2005
8. Y. R. Rashid, "Transient Failure of Zircaloy Cladding", Nuclear Engineering and Design, Vol-101, Elsevier Science Publishers B.V., North Holland, Amsterdam (1987) 305-313
9. Westinghouse Memo, "ZIRLO™ Properties for Investigation of Fuel at Byron and Braidwood, Rev. 1," MTLS-05-94, July 12, 2005
10. Westinghouse Memo, "Braidwood Unit 1 B10 Depletion and Helium Release," PPT-05-55, July 7, 2005
11. Failure Root Cause of PCI Suspect Fuel Rods from Kernkraftwerk Leibstadt (KKL) Reactor: Part 2: PIE of Failed and Sibling Sound Rods, EPRI, Palo Alto, CA, 2000. TR-111065-P2.

WARNING: This Document contains information classified under U.S. Export Control regulations as restricted from export outside the United States. You are under an obligation to ensure that you have a legal right to obtain access to this information and to ensure that you obtain an export license prior to any re-export of this information. Special restrictions apply to access by anyone that is not a United States citizen or a permanent United States resident. For further information regarding your obligations, please see the information contained below in the section titled "Export Control Restrictions."

Export Control Restrictions

Access to and use of EPRI Intellectual Property is granted with the specific understanding and requirement that responsibility for ensuring full compliance with all applicable U.S. and foreign export laws and regulations is being undertaken by you and your company. This includes an obligation to ensure that any individual receiving access hereunder who is not a U.S. citizen or permanent U.S. resident is permitted access under applicable U.S. and foreign export laws and regulations. In the event you are uncertain whether you or your company may lawfully obtain access to this EPRI Intellectual Property, you acknowledge that it is your obligation to consult with your company's legal counsel to determine whether this access is lawful. Although EPRI may make available on a case-by-case basis an informal assessment of the applicable U.S. export classification for specific EPRI Intellectual Property, you and your company acknowledge that this assessment is solely for informational purposes and not for reliance purposes. You and your company acknowledge that it is still the obligation of you and your company to make your own assessment of the applicable U.S. export classification and ensure compliance accordingly. You and your company understand and acknowledge your obligations to make a prompt report to EPRI and the appropriate authorities regarding any access to or use of EPRI Intellectual Property hereunder that may be in violation of applicable U.S. or foreign export laws or regulations.

Printed on recycled paper in the United States of America

The Electric Power Research Institute (EPRI)

The Electric Power Research Institute (EPRI), with major locations in Palo Alto, California, and Charlotte, North Carolina, was established in 1973 as an independent, nonprofit center for public interest energy and environmental research. EPRI brings together members, participants, the Institute's scientists and engineers, and other leading experts to work collaboratively on solutions to the challenges of electric power. These solutions span nearly every area of electricity generation, delivery, and use, including health, safety, and environment. EPRI's members represent over 90% of the electricity generated in the United States. International participation represents nearly 15% of EPRI's total research, development, and demonstration program.

Together...Shaping the Future of Electricity

Program:
Nuclear Power

1012915

ELECTRIC POWER RESEARCH INSTITUTE
3420 Hillview Avenue, Palo Alto, California 94304-1395 • PO Box 10412, Palo Alto, California 94303-0813 USA
800.313.3774 • 650.855.2121 • askepri@epri.com • www.epri.com